

Doctoral Thesis Summary

Preparation and characterisation of nanostructured materials for electronic gas sensor devices

Příprava a charakterizace nanostrukturovaných materiálů pro elektronická čidla senzorů plynů

Author: David John Dmonte, M.Sc., Ph.D.

Degree programme: Nanotechnology and advanced materials

Degree course: Nanotechnology and advanced materials

Supervisor: prof. Ing. et Ing. Ivo Kuřitka, Ph.D. et Ph.D.

Consultant: Ing. Pavel Urbánek, Ph.D.

External Examiners: doc. Ing. Alexandr Knápek, Ph.D.
prof. Ing. Petr Slobodian, Ph.D.

Zlín, May 2024

© David John Dmonte

Published by **Tomas Bata University in Zlín** in the Edition **Doctoral Thesis Summary**.

The publication was issued in the year 2024

Key words in Czech: *inkoustový tisk, nanočástice, ferit bizmutu, vanadičnan chromitý, senzory plynu.*

Key words in English: *ink-jet printing, nanoparticles, bismuth ferrite, chromium vanadate, gas sensing.*

Full text of the doctoral thesis is available in the Library of TBU in Zlín.

ISBN 978-80-7678-264-8

ACKNOWLEDGEMENT

To start with, I could not have embarked on this journey without the love and care of my family and friends, I am especially thankful to my parents and my sister for their financial and spiritual support towards my choice to pursue this doctoral degree and overall life.

I would also like to express my deepest gratitude to my supervisor, prof. Ing. et Ing. Ivo Kuřitka, Ph.D. et Ph.D. for the opportunity to become a member of his research team, have access to a wide range of instruments and equipment, his unwavering support throughout my doctoral research study and beyond. Besides my supervisor, I would also like to thank my consultant Ing. Pavel Urbánek, Ph.D. for his support, the insightful debates and undying motivation he had in me during this doctoral study.

Very special gratitude goes out to all members of Functional Nanomaterials Research Group at Centre of Polymer Systems of Tomas Bata University in Zlín, namely: Ing. Pavol Šuly, Ph.D., Ing. Jan Antoš Ph.D., Ing. Jakub Ševčík, Ph.D., Ing. Milan Masař Ph.D., Ing. Michal Machovský, Ph.D., Mgr. David Škoda, Ph.D., Ing. Lukáš Münster, Ph.D., Ing. Barbora Hanulíková, Ph.D., Ing. Michal Urbánek, Ph.D., Mgr. Jan Vícha, Ph.D., Raghvendra Singh Yadav Dr., Blessy Pricilla, M.Sc., Ing. Alžběta Důbravová., Ing. Monika Muchová., Hassan Ali, Ph.D., Ing. Rostislav Slobodian, Ing. Michal Macko, Ali Can Güler, MSc. and Anju, M.Sc.,

My sincere appreciation also goes to all the external collaborators from the Inorganic and Materials Chemistry Research team in University of Cologne for their passionate guidance, strategy and unrestricted admittance to key systems for this research work under Prof. Dr. Dr. (h.c.) Sanjay Mathur and specifically to the gas sensing team namely: Thomas Fischer Dr., Aman Bhardwaj Dr., Kruti K. Halankar Dr., Pelin Kavraz, M.Sc., and Ing. Ziyaad Aytuna.

It is also extremely important that I thank the team at Department of Functional Materials at the FunGlass – Centre for Functional and Surface Functionalized Glass - Alexander Dubček University of Trenčín namely Prof. Dušan Galusek, Dr.Sc. and Orhan Sisman, Ph.D., for providing their deep insight and access to equipment to complete this research work.

I am extremely thankful to the Center of Polymer Systems for the workspace, equipment, financial assistance, and facilities offered towards my research work.

This dissertation work was supported the Ministry of Education, Youth and Sports of the Czech Republic – DKRVO (RP/CPS/2022/007), the European Union's Horizon 2020 research and innovation programme under grant agreement No 739566, The ERASMUS+ programme hosted by the University of Cologne, The Mobility 2022 HR within the framework of the OP VVV project, The VEGA 1/0844/21 project granted by the Slovak Research and Development Agency, The Development of Capacity for Research and Development of TBU in Zlín, reg. no. CZ.02.2.69/0.0/0.0/16_028/0006243 and Internal Grant Agency of Tomas Bata University in Zlín, grant No., IGA/CPS/2018/007, IGA/CPS/2019/007, IGA/CPS/2020/003, IGA/CPS/2021/002 IGA/CPS/2022/002, and IGA/CPS/2023/006.

Lastly, but certainly not least, thanks to everyone who helped make this modest scientific contribution possible.

Contents

| | |
|---|----|
| Abstract | 2 |
| Abstrakt | 3 |
| 1. What are sensors? | 4 |
| 1.1 Gas sensing and the role of metal oxides | 4 |
| 2. Aim of this Doctoral Thesis Summary | 6 |
| 3. Experimental section..... | 8 |
| 4. Zinc oxide Studies | 9 |
| 4.1 Development of ZnO nanoforest based gas sensor using inkjet printing..... | 9 |
| 4.2 Sensor performance and characterization..... | 12 |
| 4.2.1 Ink development and characterization | 14 |
| 4.2.1 Gas sensing studies | 15 |
| 5. Bismuth Ferrite Studies | 18 |
| 5.1 Gas sensing schematic | 18 |
| 5.2 Material preparation | 19 |
| 5.3 Gas sensing measurement and discussion | 20 |
| 6. Chromium vanadate Studies | 25 |
| 6.1 Gas sensing system..... | 25 |
| 6.2 Material preparation | 25 |
| 6.3 Gas sensing measurement and discussion | 25 |
| 7. Summary of results and outlook | 33 |
| 8. Contribution to science and practice..... | 36 |
| References | 37 |
| List of Figures | 42 |
| List of Tables | 42 |
| List of Symbols, Units, Abbreviations and Acronyms | 43 |
| Curriculum Vitae..... | 44 |
| Research Output..... | 45 |

Abstract

In the doctoral thesis, research studies in three areas are primarily reported, Zinc oxide sensing studies, bismuth ferrite sensing studies and chromium vanadate sensing studies.

In zinc oxide sensing studies, inkjet material printing is used to print interdigitate electrodes and ultra-thin active sensing layers on various polymer thin foils and prefabricated testing sensor substrates. Hydrothermally grown ZnO nanostructures were prepared on top of printed prefabricated sensor substrates. It was utilized for preliminary gas sensing in a custom gas testing system towards selected target gas (ethanol vapours).

In bismuth ferrite sensing studies, the nanomaterial and its doped version using strontium was prepared using sol-gel method. The material was characterized and gas sensing measurements like cross-testing was also performed with a group of selected gases, and the linearity of the calibration curve was demonstrated towards the target gas within the verified concentration range. It was tested for selectivity, relative response, sensitivity, repeatability, response, and recovery times towards selected target gas NO_2 . The plausible sensing mechanism was discussed.

In chromium vanadate sensing studies, the nanomaterial was prepared using the co-precipitation method. The material was then characterized by all In-house characterization techniques. Cross-testing was also performed with a group of selected gases, and the linearity of the calibration curve was demonstrated towards the target gas within the verified concentration range. It was tested for selectivity, relative response, sensitivity, repeatability, response and recovery times towards selected target gas NH_3 . The plausible sensing mechanism and band bending study were discussed.

To summarize, despite preliminary achievements in digitally printed devices, a simpler fabrication technique was finally adopted to prepare gas sensors based on original nanostructured materials. The work succeeded in preparing sensors with reasonable sensitivity, selectivity, and response repeatability towards electron-withdrawing and electron-donating gasses represented by NO_2 and NH_3 , respectively. Moreover, even without using noble metals in the structure of the sensor samples, the sensors demonstrated at least comparable or better parameters than their analogues reported in contemporary literature.

Abstrakt

Disertační práce se věnuje především tématům výzkumných studií ve třech oblastech: studie senzorky oxidu zinečnatého, studie feritu bizmutu a studie oxidu zinečnatého a vanadičnanu chromitého.

Ve studiích snímání oxidu zinečnatého, materiálový tisk použit pro přípravu interdigitů a ultra tenkých aktivních sensorových vrstev na různé tenké polymerní fólie a prefabrikované sensorové substráty. Na těchto substrátech byly připraveny ZnO nanostruktury pomocí hydrotermálního růstu. Odezva těchto struktur na vybraný plyn (páry ethanolu) byla měřena v testovacím systému vlastní konstrukce.

Při studiu senzoru z feritu bizmutu byl metodou sol-gel připraven nanomateriál a jeho verze dopovaná stronciem. Materiál byl charakterizován a byla také provedena měření pro snímání plynů, jako je křížový test, se skupinou vybraných plynů a byla prokázána linearita kalibrační křivky vůči cílovému plynu v ověřovaném koncentračním rozsahu. Byla testována selektivita, relativní odezva, citlivost, opakovatelnost, odezva a doby zotavení vůči vybranému cílovému plynu NO₂. Byl diskutován pravděpodobný mechanismus snímání.

Při studiu snímání vanadičnanem chromovým byl nanomateriál připraven metodou koprecipitace. Materiál byl poté charakterizován všemi vlastními charakterizačními technikami. Bylo rovněž provedeno křížové testování se skupinou vybraných plynů a byla prokázána linearita kalibrační křivky vůči cílovému plynu v ověřovaném koncentračním rozsahu. Byla testována selektivita, relativní odezva, citlivost, opakovatelnost, doba odezvy a výtěžnosti vůči vybranému cílovému plynu NH₃. Byl diskutován pravděpodobný mechanismus snímání a studie ohybu pásma.

Souhrnem, i přes počáteční úspěchy v oblasti digitálního tisku elektroniky byla nakonec zvolena jednodušší metoda přípravy sensorů plynů založených na originálních nanostrukturovaných materiálech. Byly úspěšně aplikovány v senzorech vykazujících přiměřenou senzitivitu, selektivitu a opakovatelnost odezvy na elektron akceptorní a elektron donorní plyny, reprezentované NO₂ a NH₃. Připravené vzorky sensorů se i bez použití drahých kovů vyznačovaly alespoň stejně dobrými nebo lepšími parametry než jejich obdoby popisované v současné literatuře.

1. What are sensors?

Any device which provides a measurable change in response to a specific physical quantity is called a sensor. There are many types of gas sensors and have been an integral part of many products. They are an important auxiliary component for a larger purpose allowing more control. For example, oxygen sensors dominated the automobile market being extensively used in every combustion engine. They are going to play a major role in a smart era where smart machines and humans coexist in a connected world such as wearable electronics, medical care, space exploration and Internet of things[1–6]. Smart materials have revolutionized the way we think about the possibilities of materials science and engineering. These materials, which have the capability to sense and respond to changes in their environment or stimuli from various sources such as optical, electrical, magnetic, mechanical, thermal, and chemical signals, have helped us to move closer to the goal of creating systems that can self-adapt, self-diagnose, and self-respond. This type of technology can be seen as an artificial imitation of intelligence, allowing us to create systems that can learn and adapt over time, much like a living organism[7–14].

1.1 Gas sensing and the role of metal oxides

The development of advanced gas sensors to have high selectivity, sensitivity, fast response / recovery speed is extremely necessary as it can play significant roles in environmental monitoring, military affairs, automotive, healthcare, industrial requirements etc[15–17]. An essential problem that most metropolitan areas is going to have to deal with would be ambient air quality, which affects both human health and the environment. While stating that "91% of the world's population live in locations where air quality exceeds WHO guideline limits," the World Health Organization (WHO) notes that "low air quality causes more deaths yearly than HIV/AIDS and malaria combined." More and more individuals are developing illnesses including strokes, chronic pulmonary diseases, lung cancer, etc. because of inhaling air with high amounts of pollution, which leads to 7 million premature deaths annually [18].

Sensor technology, according to Simon et al., is one of the prominent technologies soon, with rapidly growing applications in both the industrial and private sectors [19]. An interaction of adsorbed molecules with specific surface sites or active species present on the surface is responsible for the change of concentration of charge carriers in the active layer, which is macroscopically manifested as change in overall conductivity/resistance values. These changes are directly related to concentration of detected analyte if the sensing material has perfect selectivity. With the rest of all other factors in a controlled non-interfering condition. Therefore, gas sensors are of main interest in this thesis, because of their simplicity and ease in terms of operation and fabrication[20–22]. This sensing interest in the scientific community has created a need for intense research with the

aim to deliver room temperature gas sensing using nanostructures for example such as carbon nanotubes (CNT's)[23,24]. Therefore, it is of essential need to explore new gas sensing materials and novel nanostructures to help achieve the much needed requirement of a sensor with high sensitivity, low working temperature, and simple preparation methods.

Metal oxide semiconductors (MOS), one of several gas sensing materials, outperform other sensors in terms of performance because to their exceptional physical and chemical characteristics and distinctive structure. Since these materials have a large band gap, they can exhibit the whole range of electrical characteristics. The material size frequently has a significant impact on the MOS's characteristics and is capable of a wide detecting range as shown in Figure 1.1. An effective gas sensing material, for example must show electrical characteristics that undergo large shifts. From a commercial standpoint, low-cost and simple manufacturing processes are also significant factors that contribute to this material's appeal [25].

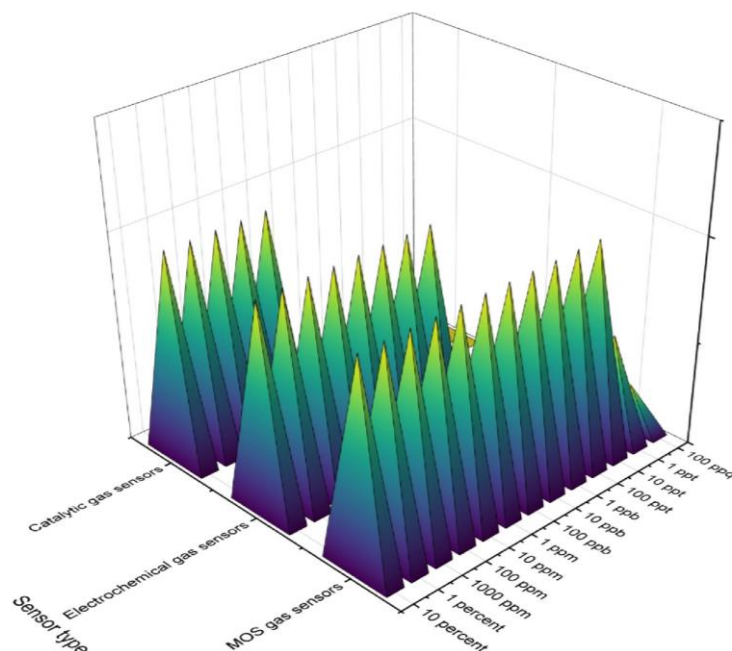


Figure 1.1: The gas concentration detecting range of many typical gas sensors.

It traditionally used to be dominated single metal oxide such as Zinc oxide, Tin oxide. They are comparatively easier to prepare and are known to be stable in the long term. They were usually doped to help improve selectivity, stability, etc This slowly transitioned out to bimetallic oxides which offer more control due to their synergistic effects between the two metals such as improved catalytic properties, variability etc. Certain structures such as spinel AB_2O_4 are then of high interest as they can provide more ability oxygen vacancies to improve sensitivity and stability for applications such as gas sensing. Another interesting structure which has been is Perovskite ABO_3 . This structure has been of trending interest in many fields of applications as the ability to modify atomic sites, there by adjusting the electric dipole and give rise to properties like ferroelectricity.

2. Aim of this Doctoral Thesis Summary

In accordance with its title, this work focuses on the preparation and characterization of new nanostructured materials as transducers for electronic gas sensor devices, specifically chemiresistive sensors of various gases with the intention of surpassing the state of the art in their sensitivity. Moreover, there is an intention to avoid using expensive noble metals in the material synthesis. It means the new sensors should demonstrate at least comparable, or preferably better, parameters than their analogues reported in contemporary literature. To achieve this aim, one main goal and one secondary goal have been defined:

- A) To prepare sensor samples with reasonable sensitivity, selectivity, and response repeatability towards:
 1. solvent vapours represented by ethanol,
 2. electron-withdrawing gasses represented by NO₂,
 3. electron-donating gasses represented by NH₃.
- B) Besides that, adaptation of state-of-the-art methods or further development in material synthesis is to be performed to find new ways, modifications or applications of the necessary preparation techniques which also may deliver new results.

Note, both goals include selection of suitable materials for preparation of the sensors, as their choice is principally limited by the nature of the interaction between the analyte and the sensing material, and practically limited by the available technologies considered with respect to the processability of the selected materials, and by the availability of appropriate testing apparatuses.

The following objectives are necessary to achieve the goals of this work. The objectives are structured according to the sub-divisions of the main goal, labeled as Goal A, while the achievement of the secondary goal, labeled as Goal B, is incorporated across the three sections wherever appropriate.

❖ Ethanol vapours sensing – zinc oxide:

This part of the work focuses on the development of gas sensors using specific methods and inkjet printing material depositing systems to develop the nanostructured zinc oxide materials for sensing of ethanol and eventually other vapours of organic solvents. It is based on the previous expertise of my predecessors in the research group of Nanomaterials and advanced technologies. The goal can be achieved by stepwise accomplishment of the following objectives:

- Mastering of the inkjet printing system for printing of printed silver interconnects, electrodes, electrical components using silver nanoparticle-based inks on all required substrates ranging from polymers, glass to ceramic.

- Research and development of metal oxide-based nanoparticle ink to deposit on fabricated or prefabricated sensor platform for nanomaterial growth for selective gas sensing in ambient air. Prepared nanostructures shall be characterised by in-house available analytical methods.
- Evaluation of the response to the presence of EtOH gas at room temperature in a custom-built gas sensing system to build a pathway for developing an advanced sensing device.

❖ NO₂ sensing studies – bismuth ferrite:

This part of the work focuses on the development of gas sensors using strontium doped bismuth ferrite materials for very low concentration detection of NO₂ gas. The shift towards this material and the simplification of the preparation technology are based on experience gained from the work on the sensing of ethanol using zinc oxide transducer, which was not as successful as initially expected. The goal can be achieved by stepwise accomplishment of the following objectives:

- Preparation and study of bismuth ferrite metal oxide nanostructures and strontium doped bismuth ferrite for selective gas sensing in synthetic air. Prepared nanomaterials and nanostructures shall be characterised by in-house available analytical methods.
- Improvement of the gas sensing system to enhance measurements of cross-selectivity, repeatability, stability, and sensitivity in various conditions.
- Systematic evaluation of the response to the presence of NO₂ gas flow in a custom-built gas sensing system to finalize in developing an advanced sensing device.

❖ Ammonia sensing studies – chromium vanadate:

This part of the work focuses on the development of gas sensors using chromium vanadate materials for low concentration detection. It is a continuation in the successful line of the research enabled by the NO₂ studies. This goal can be achieved by stepwise accomplishment of the following objectives:

- Preparation and study of chromium vanadate for selective gas sensing in synthetic air. Prepared nanomaterials shall be characterised by available analytical methods.
- Improvement of the gas sensing system to enhance measurements of cross-selectivity, repeatability, stability, and sensitivity in various conditions.
- Systematic evaluation of the response to the presence of NH₃ gas flow in a custom-built gas sensing system to finalize in developing an advanced sensing device.

3. Experimental section

The work was performed partially in the laboratories in the Centre of Polymer Systems in the Tomas Bata University in Zlín and partially in the Inorganic Chemistry laboratories of the Department of chemistry in the University of Cologne. Additional key measurements were performed at the FunGlass – Centre for Functional and Surface Functionalized Glass in the Alexander Dubček University of Trenčín, Slovakia.

The research work in this thesis has three parts oriented on three representative metal oxide materials. The first part was zinc oxide with the focus on nanomaterial growth and inkjet printing. The second part was focused on Bismuth ferrite and its doping to improve its sensing properties towards NO₂ and the third study was focused on Chromium Vanadate and its sensing properties towards NH₃.

Here, the list of materials and methods used throughout the work,

In Zlín, the silver nanoparticle-based inks such as silver dispersion (50 – 60 wt%) from Sigma Aldrich was selected for printing on Microscope glass slides (Thermofisher scientific), polymeric foils like Polyimide foil Upilex - 50S (PI) from Ube industries, Japan and other prefabricated substrates The prefabricated sensor platform Interdigitated gold electrodes BI2 from Tesla Blatná

The FUJIFLIM Dimatix-2800 series material inkjet printer was used to deposit these inks. It features 16 nozzles with a 21.5 µm nozzle pitch and two distinct types of Dimatix DMC-11610 ink cartridge printheads. The first type allows for 10 picoliter drops, while the second type simply differs in that it ejects 1 picoliter drop. The waveform configuration and permitted voltage for each nozzle in the printing head regulate the fluid ejection operation. The former type is only used in our work.

For the nanomaterial growth, The first step of the seed layer ink required Zinc acetate dihydrate- Zn (CH₃COO)₂ from Penta chemicals, UV spectroscopy grade ≥ 99.8 % ethanol (Penta chemicals), BYK 348- Silicone surfactant for aqueous coatings, printing inks from BYK, Germany to improve ink stability. It has been characterized at 25 C. The surface tension was determined with a Krüss K100 force which uses the Wilhelmy plate methodology. The viscosity of dispersions was measured by a Ubbelohde type viscometer. The density was determined by pycnometry. The second step for the hydrothermal growth solution, zinc nitrate hexahydrate Zn(NO₃)₂·6H₂O (98.0%) from Sigma Aldrich and hexamethylenetetramine (CH₂)₆N₄ (99.6%), from Lachner, and polyethyleneimine (molecular weight 800) from Sigma Aldrich was used. The additional PTMSDPA poly[1-phenyl-2-[p-(trimethylsilyl)phenyl]acetylene] was also procured from Sigma Aldrich .The specific description about the experimental condition , characterization and setup for gas sensing along with other related details are explained in detail in their respective chapter below.

In Cologne, The material bismuth ferrite and it's doped variant was prepared by using a modified pechini method using a metal citrate complex along with a polymerizing agent: ethylene glycol. This remaining gel is sintered at 700 °C in air for 4 hours with 5°C/hour heating rate and cooling rate in a Gero Eurotherm tube furnace in air. The materials. $\text{Bi}(\text{NO}_3)_3 \cdot 5\text{H}_2\text{O}$, $\text{Fe}(\text{NO}_3)_3 \cdot 9\text{H}_2\text{O}$, $\text{Sr}(\text{NO}_3)_2$, nitric acid, citric acid and ethylene glycol(50% aqueous solution). were all acquired from Thermo Fisher Scientific Inc., United States. The material chromium vanadate was prepared by using chromium nitrate and ammonium metavanadate and ethanol (99.8%) were also acquired from Thermo Fisher Scientific Inc., United States. and DI water from laboratory water treatment system. Then in equimolar amounts of precursor solution blended, the resulting co precipitate was washed and then the precipitate is sintered at 600 °C in air for 4 hours with 5°C/hour heating rate and cooling rate in same tube furnace mentioned above in argon flow to prevent any reaction with oxygen. The specific description about the experimental condition, characterization and setup for gas sensing along with other related details are explained in detail in their respective chapter below.

In Trenčín, the chromium vanadate material was characterized by XPS - X-ray photoelectron spectroscopy to have an in -depth surface analysis for understanding the material property and possible mechanism. The detail explanation is given in their respective chapter.

4. Zinc oxide Studies

4.1 Development of ZnO nanoforest based gas sensor using inkjet printing

First, the prefabricated sensor platform Interdigitated gold electrodes BI2 from Tesla Blatná is placed for UV-OZONE treatment for 10 minutes to enhance its wettability and increase surface energy[26,27] and will be further mentioned as substrate A and substrate B. The polyimide foil Upilex-50s was cleaned and dried in the oven. After which, it was pretreated similarly as before ZnO seed layer coating. In case, of the polyimide foil, the Silver dispersion was filtered through a 0.22 micrometre pore syringe filter before it was injected inside a cartridge to be used to print the selected motif of the interdigit on the polyimide foil or the substrate. Several various designs of the interdigit were designed with 40 dpi according to our need to avoid contact with metallic components and smooth integration with our electronic clips for resistance measurements. This was further cured at 250 °C for 1 hour to remove all capping agents and polymeric solvents and after cooling is shown in Figure 4.1.

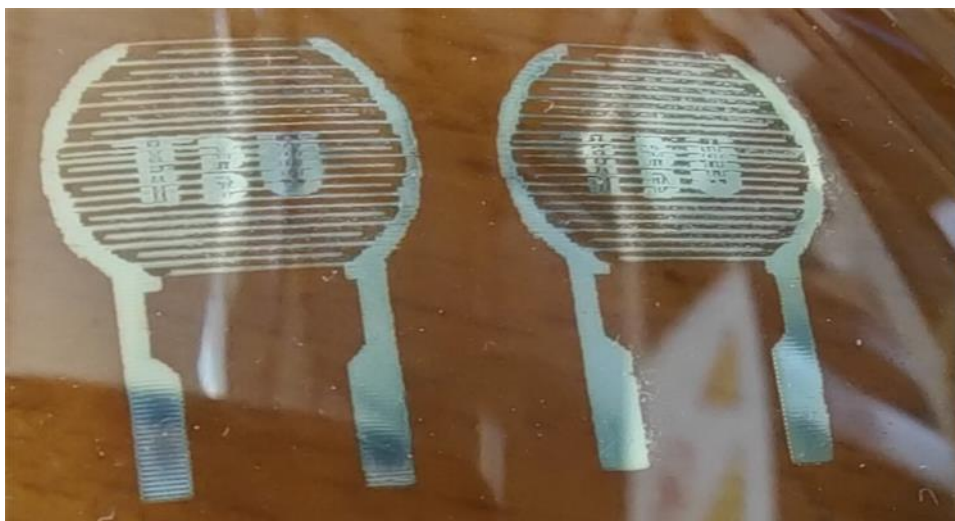


Figure 4.1: Inkjet printed Interdigit on polyimide foil for gas sensing.

The ZnO seed layer Ink was prepared in the form of dispersions. Zinc acetate dihydrate $Zn(CH_3COO)_2$ was dissolved in UV spectroscopy grade $\geq 99.8\%$ ethanol at $50\text{ }^\circ\text{C}$ for 1 hour on stirring till it forms a 10 mM clear dispersion without any sediment particles. After, cooling, using the dropper, one drop of BYK 348 is added to the ink. It was then filtered through a 0.22 micrometre pore syringe filter before filling the cartridge and then printed onto (i) Fabricated electrode structures on flexible polyimide foil and (ii) clean prefabricated gold interdigitated alumina substrates.

After deposition, it was cured at $500\text{ }^\circ\text{C}$ for 10 minutes in a muffle furnace (Nabertherm, Germany) to remove solvent and allow for a strong bonding between the seeded nanoparticles and the substrate. Then, these substrates were subject to different concentration of hydrothermal growth kept in position in a blended solution of Zinc nitrate hexahydrate, polyethyleneimine, hexamethylenetetramine and double distilled water branched at $95\text{ }^\circ\text{C}$ for different periods of time as shown in the Table 1 below[28].The concentration of PEI varies as to control nanorods aspect ratio and to infer if there is any plausible change in its conduction properties. It was then later taken out, cleaned using distilled water and allowed to be dried before being tested. Then a quick heat treatment of high temperature for 10 – 15 mins, which is then cooled and lastly the heat treatment is employed by using a hotplate at $80\text{ }^\circ\text{C}$. After which the sensor is ready for testing.

A microscopic image of the final sensors is shown, along the polyimide foil undergoing a bending test in Figure 4.2. After required zinc nanoforest growth is similarly grown. For preliminary response comparison, 1 % polymer PTMSDPA ink with ethanol is tested for efficient printing and used as a additional layer for testing its influence on sensing activity. A usable waveform will be created along with proper ejecting voltage. This ink is then inkjet printed for 3 layers onto the interdigit on the selected sensor platforms and are allowed to dry before being tested. It is seen in the middle of the Figure 4.3. All the sensors developed were characterized by in-house techniques and are discussed in detail in the thesis.

Table 1 ZnO Nanorods growth solution (PEI concentration varies for control)

| Precursors (0.05M) | 500 ml (6 hour) | 1000 ml (2 hour)) |
|--|-----------------|-------------------|
| Zn(NO ₃) ₂ ·6H ₂ O | 7.43 g | 14.875 g |
| HMTA | 3.505 g | 7.00 g |
| PEI | 5.6 g [0.016M] | 5.6 g [0.008] |



Figure 4.2:(a) Schematic of prefabricated sensor and interdigit motif for sensor (above) (b) coated ceramic and flexible inkjet printed sensor before and after growth (below)

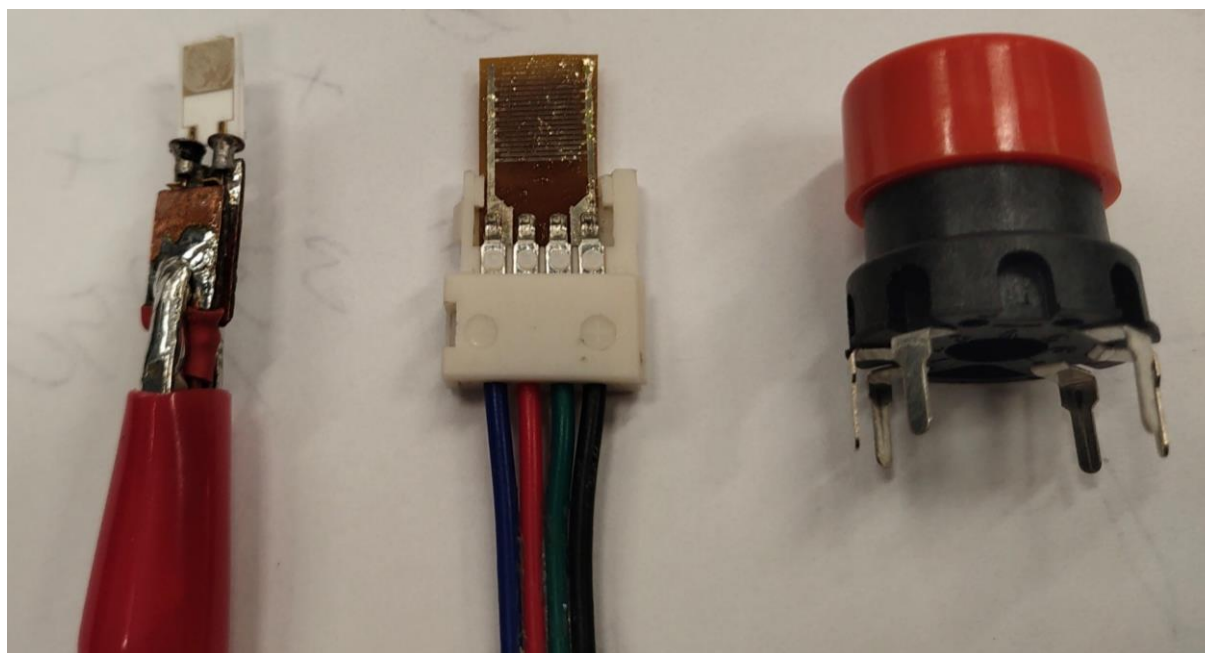
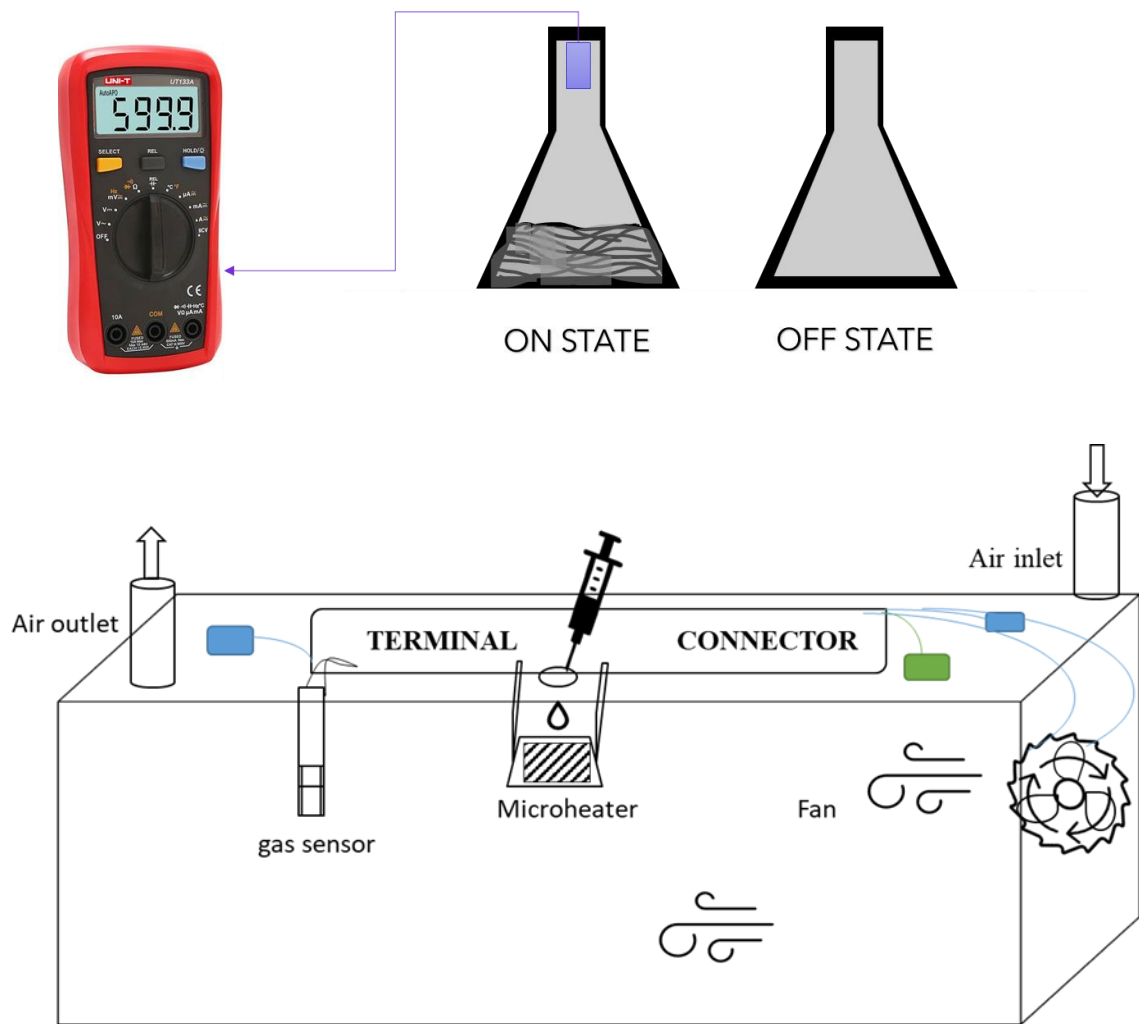


Figure 4.3: The sensors (left to right) Ceramic fabricated sensor, flexible substrate and a reference sensor with the required electronics.

4.2 Sensor performance and characterization

Response of sensors having different growth conditions of ZnO nanoforest was measured using the Multimeter UNI-T HC-UT71D with interface software that records and observes resistance. The sensors have been studied under SEM for topographical changes among the variants. These sensors first go through an “ON/OFF “testing phase to confirm sensor exposure to vapours of ethanol and also recovery time when it is immediately removed from any vapours as shown in . All the experiments were carried in ambient atmosphere in the laboratory. Response of the sensors were measured at room temperature with no additional heating or optical energy source in a custom built gas sensing measurement setup as schemed in Figure 4.4.

Synthetic air was used as a carrier gas at 200 ml/min to remove the presence of any other interference possible from competing gases. This gas flow was controlled by mass flow controller EL-FLOW Prestige (Bronkhorst High Tech BV, Netherland). The calculated amounts of ethanol were dropped on the surface of the micro heater, through a rubber cap which would be instantly evaporated due to the high temperature. The fan in the back of this closed box mixes the air and therefore, it reaches the sensor, which is either connected through the terminal block via header pins to the 2- pin holder for prefabricated sensor. Similarly, another set of header pins connect via the terminal block using the 4-pin connector for the polyimide based flexible sensors. There are three K-type temperature sensors, two are depicted as blue squares on the lid of this box, connected the main terminal board to monitor temperature through the experiment. The other green one is kept near to center to monitor the overall temperature. The fan was turned off as it produced a lot of static noise in the resistance readings to be monitored for the preliminary testing. Another two pins present in the terminal is for powering the LED which is fixed on a 3-D printed holder for the prefabricated sensor to maintain light and power exposure for improved conductivity and response in the later stages of testing. The resistance changes of the sensor devices are measured and logged using the multimeter UNI-T HC-UT71D with interface software.



External View

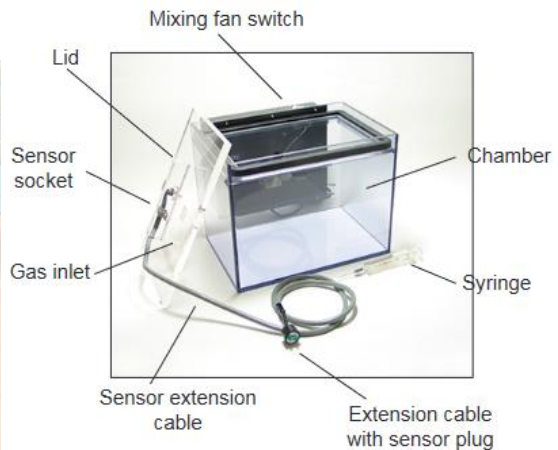
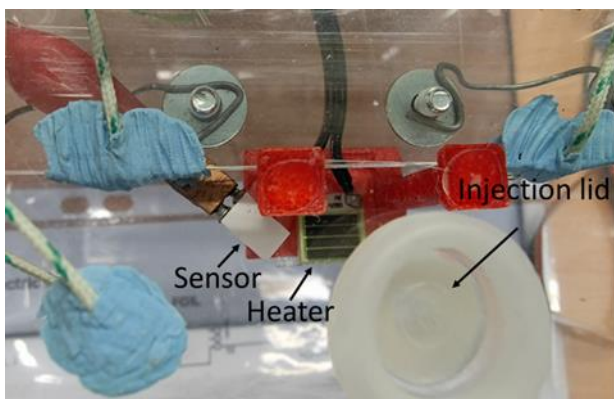


Figure 4.4: (Top to bottom) “ON/OFF” testing by alternating between a beaker with saturated ethanol vapours and an empty beaker, Schematic of the gas sensing chamber and an image of the lid (overview)

4.2.1 Ink development and characterization

The ink composition for the ZnO seed layer was characterized at 25 °C. This ink was experimentally developed within the space of parameters by trial and error until satisfactory performance of the process was achieved. The dimensionless values are calculated for the respective values and shown in Table 2. The three dimensionless constants are: Ohnesorge number, that describes the tendency for a drop to either stay together or fly apart, by comparing viscous forces with inertial and surface tension forces, while the Reynolds number is the ratio of inertial forces within a fluid, used to determine the flow pattern as laminar or turbulent. On the other hand, Weber's number is used to analyse fluid flows especially in interfacial conditions.

Table 2 Seed layer ink properties and generated dimensionless values

| Viscosity | Density | Surface tension |
|-------------------|-----------------------------|---------------------|
| (2.0 ± 0.1) mPa-s | (785 ± 1) kg/m ³ | (22.27 ± 0.01) mN/m |
| Reynolds number | Weber number | Ohnesorge number |
| 44.2 | 21.7 | 0.1 |

Using the calculated values, by substituting the Reynolds and Weber numbers for the formulated ink in the dimensionless formulation space graph which is based on Prof Brian Derby research[29]. It can be clearly seen in Figure 4.5 that the ink marked by the pink circle is in the sweet zone which is marked green. The area on the right is characterized by $Z > 10$, where generally satellite drops are likely to dominate the printing process and the area to the left characterized by $Z < 1$, is where the ink is too viscous for printing. However, on modification of the double impulse waveform, it has shown to generate fairly good quality droplets as seen in Figure 4.5. This confirms that the ink will perform well.

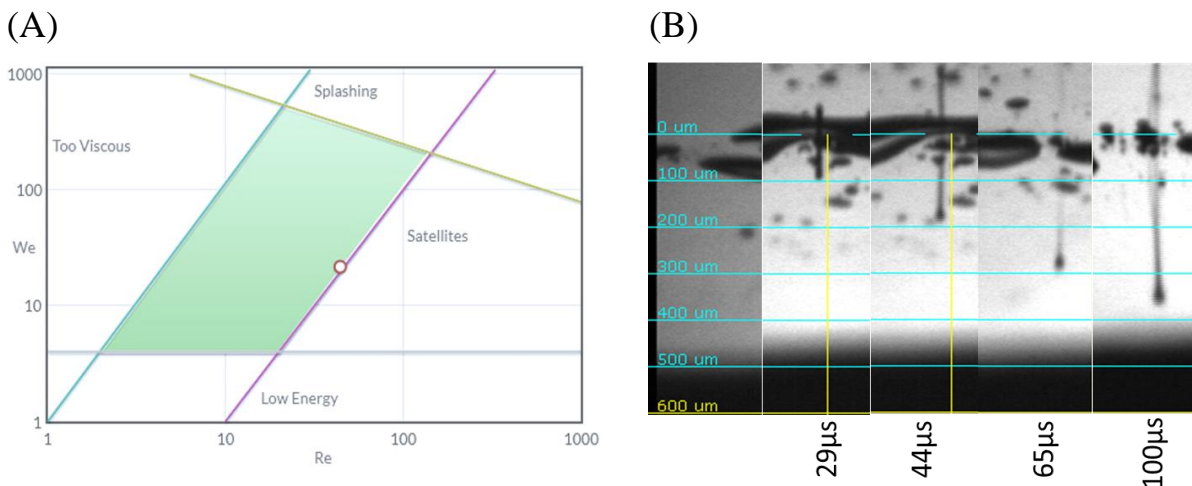


Figure 4.5: Inkjet formulation space graph using Reynolds and weber numbers based on [29] Brian Derby(A) Droplet formation as seen from the fiducial camera (B).

4.2.1 Gas sensing studies

Substrate A

In terms of gas sensing, the relative responses by sensor substrate A can be seen in the Figure 4.6. In the first figure, it can be observed that the on/off testing shows a very rapid response and recovery towards saturated vapours of ethanol to be around 5.87 % while being placed near the mouth of the beaker. This seems to relate to expectation as it had no additional source of energy such as heat or optical or force. These substrates were then moved to the box for further testing. After attaining a baseline, periodic drops of 100 μ l ethanol is being dropped on the microheater set to 120 °C. Considering all the ethanol dropped onto the microheater evaporated uniformly and considering the flow to air to be minimum yet overlooking diffusion models, we calculate the amount of ethanol in the chamber to be 7800 ppm at maximum. It shows a very minimum relative response and recovery times of over 3 minutes and at least 8- 10 minutes to return to baseline.

However, the mediocre repeatability as can be seen in Figure 4.6 the red arrows show the injection of ethanol and response was consistent for over 6 cycles of exposure over a time of 65 minutes. The reduction of relative response in terms of resistance could be attributed to the reduced concentration of the gas analyte and the lack of energy for the oxygen on the surface of our sensor to promote absorption. The only flow of electrons though the interdigit was multimeter used to record the resistance. The multimeter is a resistance weighted electrical measurement device, so, we assume it's influence on the interdigit should be very minimal or negligible.

Substrate B

The gas sensing response for the 6 hours ZnO growth nanoforest growth sensor is show in Figure 4.7. It can be clearly seen that, there is consistent response to vapours of ethanol. The amount of ethanol is kept the same 100 μ l and is again evaporated on the microheater inside in the chamber, c.a 7800 ppm. The red arrows are when the ethanol is injected on the microheater for it to be evaporated. There is a clear spike in resistance within 3 minutes on average, which shows fast response time. This peak then settles down in 8 to 10 minutes, which is considerably a faster recovery time. It is clearly capable of efficient repetitive sensing, although the sensitivity can maybe be further improved with optimization. The coexisting gases of uncontrolled ambient air is experienced regardless to recalibration of the sensor, is the reason for the baseline drift. Several structural factors and room temperature sensing generally require a longer time for desorption and diffusion of vapor molecules. Low temperature sensing mechanism cannot be well explained by established models. Hence, there is still a need of an explanation for this sensing action. The preliminary gas sensing for PTMSDPA poly[1-phenyl-2-[p-(trimethylsilyl)phenyl]acetylene] which is a known conductive polymer for its interesting gas permeation and sorption properties[30]. A 1% of the polymer solution is then drop casted on ZnO nanoforest sensor In

Figure 4.8, the red arrows are when the ethanol is injected on the microheater for it to be evaporated. It shows a similar but decreased sensing characteristics, unstable response, and sensitivity. It also shows slow recovery and is not efficient at repeatability. More research needs to be done to be further enhance the gas sensing ability. The sensor suffers from poor kinetics and lack of energy. The saturation ability of the air flow to desorb the ethanol gas molecules back from the surface of the nanomaterial seems to also not be sufficient.

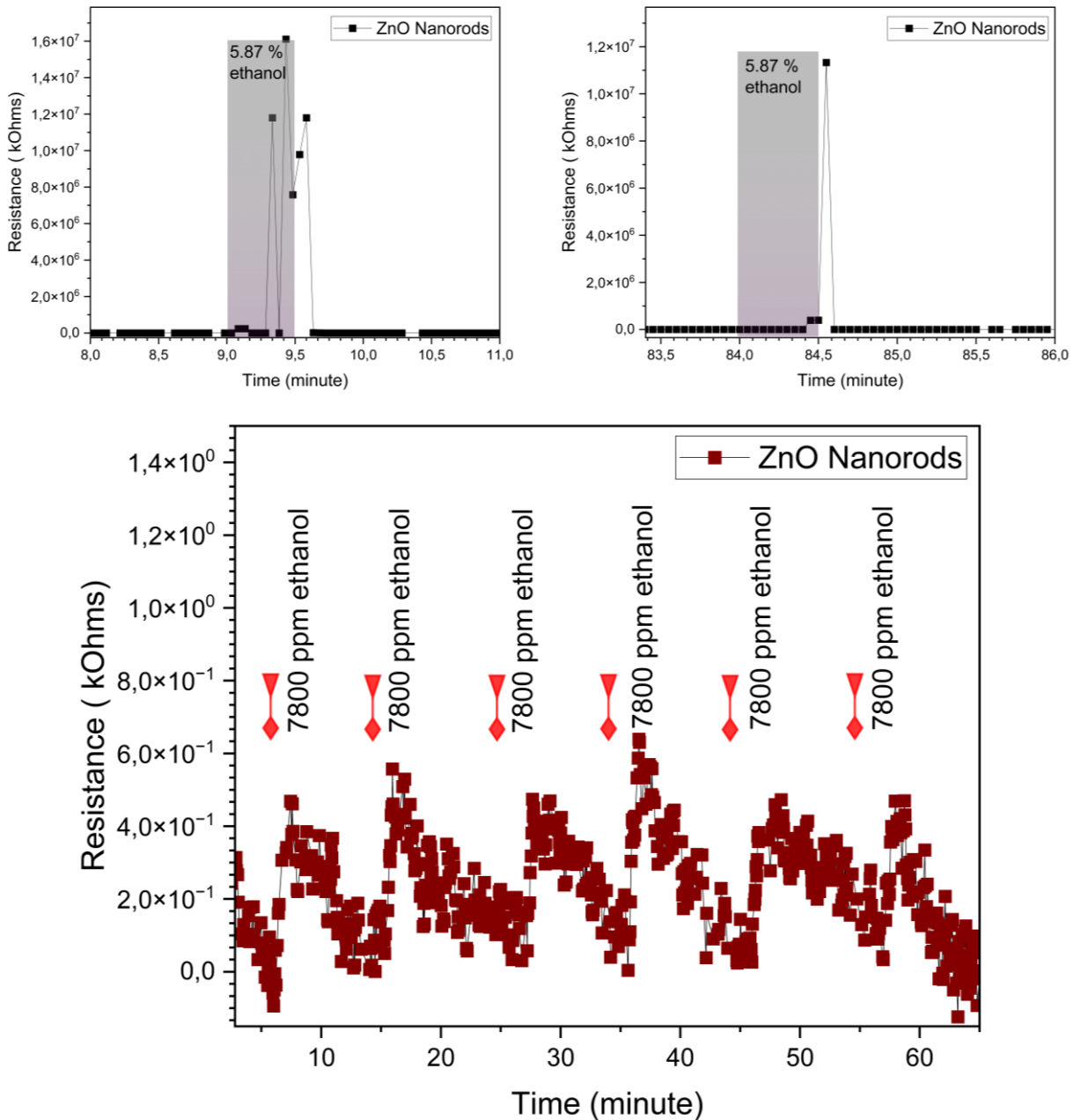


Figure 4.6: Gas sensing responses from the on/off testing (above) and gas chamber testing (below).

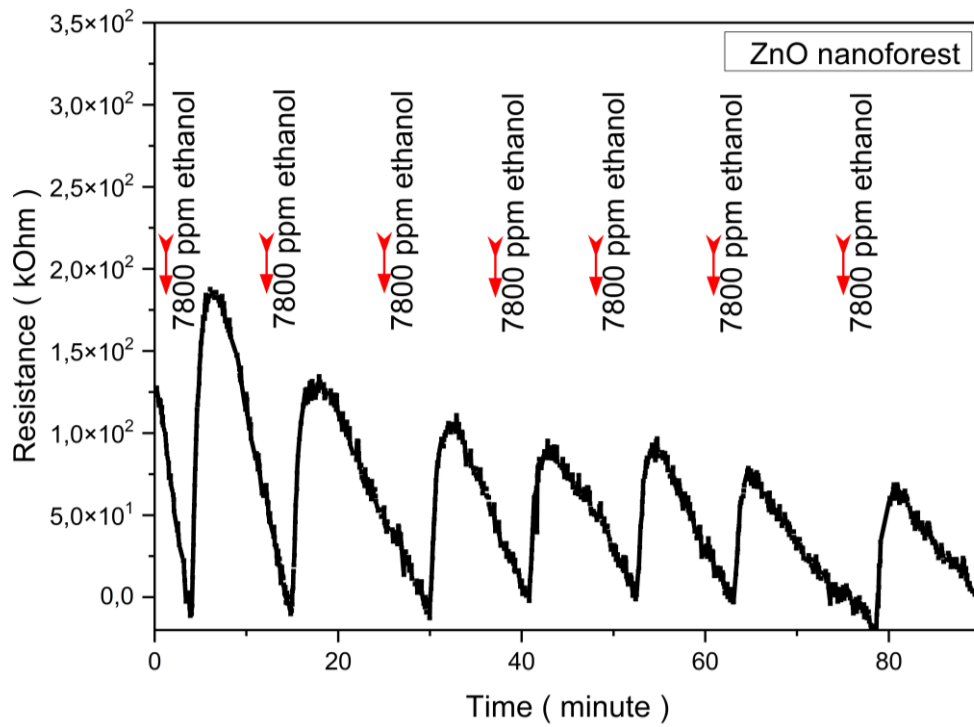


Figure 4.7: Observed gas sensing responses for ZnO nanoforest sensor.

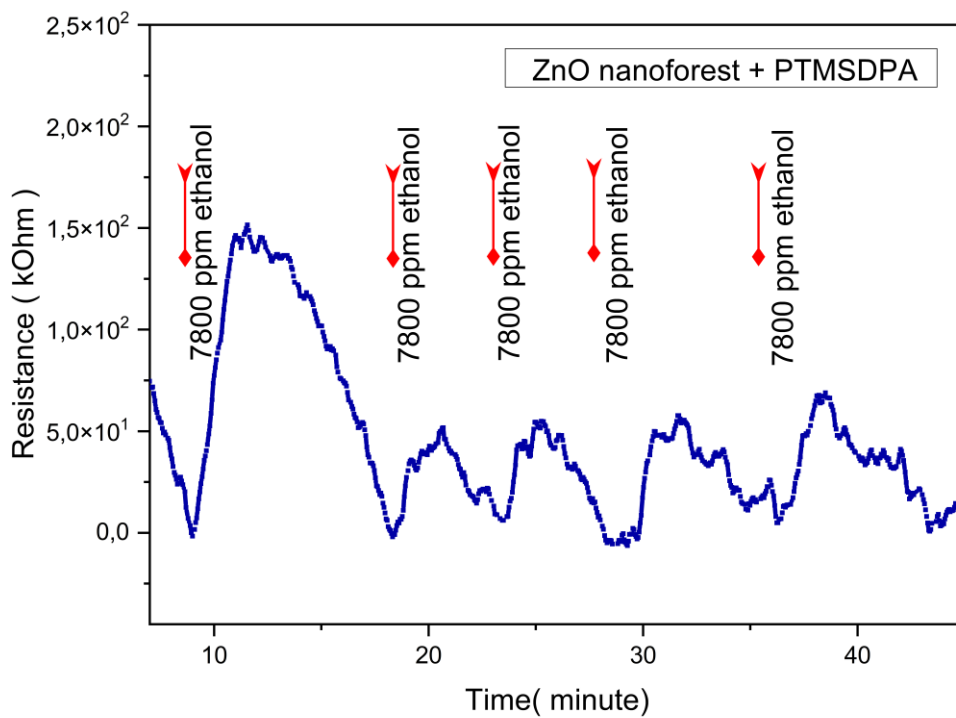


Figure 4.8: Observed gas sensing responses for polymer drop casted sensor.

5. Bismuth Ferrite Studies

5.1 Gas sensing schematic

In a distinctive setup, gas sensing measurements were examined in a 250 ml airtight chamber with a provision for gas injection and exhaust. Figure 2 illustrates this design, and the desired concentration (in ppb and ppm) was reached by combining the analyte gas flow with the synthetic air gas flow while employing two mass flow controllers (Aera FC-7700C) at the same time. The background environment was created using a dry air gas cylinder (Air Products and Chemicals, Inc., certified for 0% humidity) to rule out any surface interactions with moisture. For dilution in the measurements, target gases (NH_3 , NO_2 , CO , CH_4 , and $\text{C}_2\text{H}_6\text{O}$) in certified gas cylinders are utilized. Using a Keithley K2700 for data acquisition, the resistance to exposure to air and mixtures of analytes is continually measured from the sensor. For precise heating, a calibration curve between voltage and temperature is created using custom programs created in LabVIEW. The heater voltage was around $30 - 35 \Omega$ as standard, which meant the microheater is functional.

The recommended maximum voltage for sustained usage was rated to be upto 15 V and optimally only set to allow only upto 500 milliamps. Even if the microheater is constituted of titanium, it is not recommended to be used at high voltages/temperature for extended periods of time. It was powered by the Elektro Automatik power source meter, model (ES-PS 3065-03B). A custom designed 4 pin connector for two sensors was soldered, but only one was used to connect the sensor to the required electronics in the chamber as shown along with the schematic and sensing chamber in the Figure 5.1. The sensitivity/relative response for the following work uses the formula:

$$S = \frac{Ra - Rg}{Ra} \quad (1)$$

$$S = \frac{Rg - Ra}{Ra} \quad (2)$$

For reducing gases, use equation (1), while for oxidizing gases, use equation (2). Rg and Ra stand for the sensor's resistance to analyte presence and its resistance to synthetic air, respectively. The terms T-90 response and T-90 recovery time refer to the amount of time required for the sensor to saturate to 90% of the total resistance [31–33].

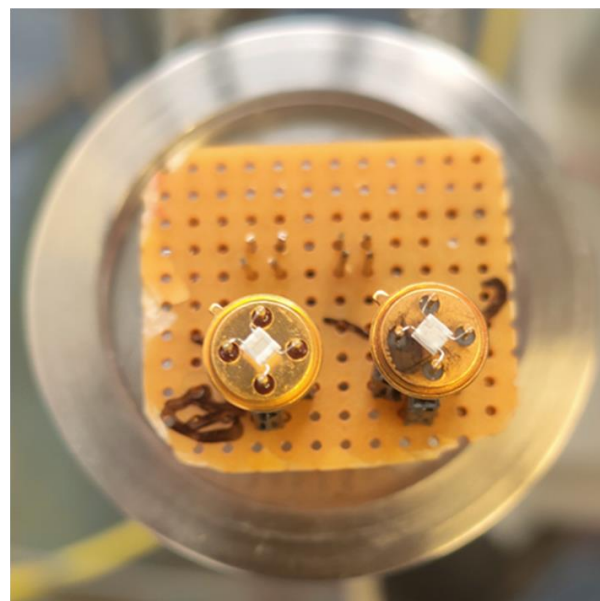
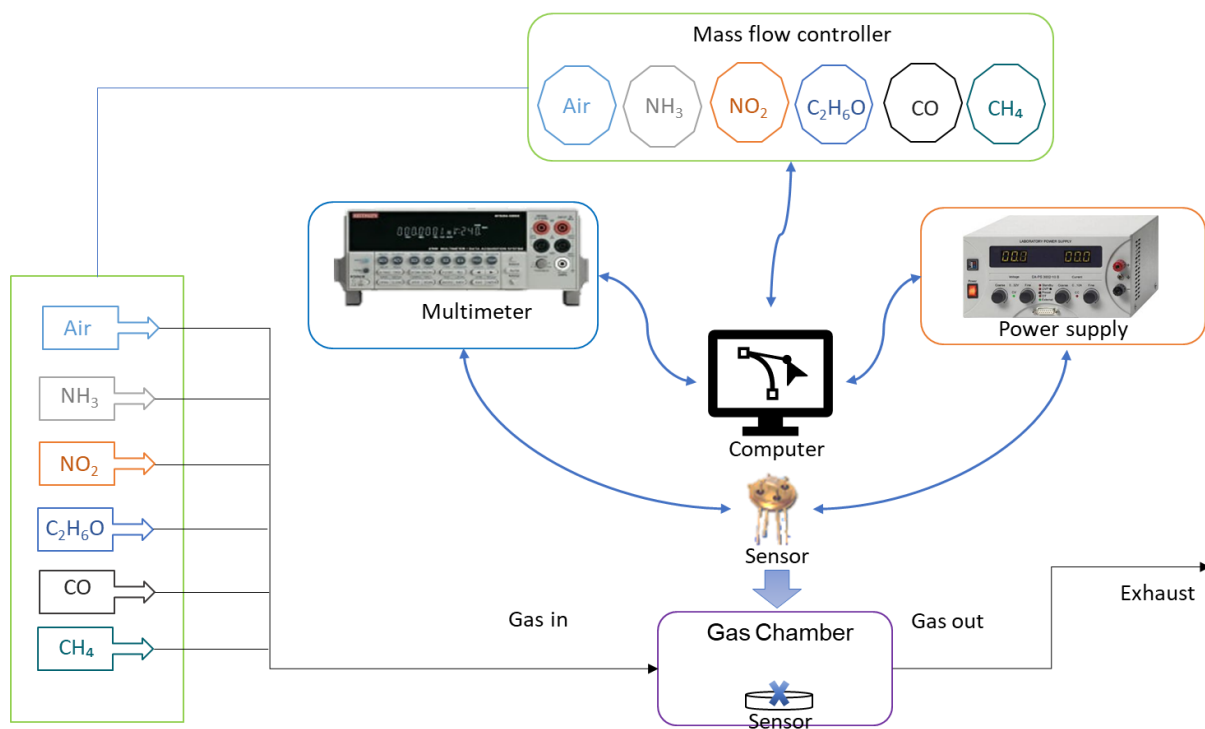


Figure 5.1: Schematic of the gas sensing system (above) and the sensing chamber with the sensor holder with the chamber lid (below).

5.2 Material preparation

In this work, a sol-gel approach was employed to synthesis $\text{Bi}_{1-x}\text{Sr}_x\text{FeO}_3$ ($x = 0, 0.20$). This method was slightly modified [34]. $\text{Bi}(\text{NO}_3)_3 \cdot 5\text{H}_2\text{O}$ In diluted nitric acid, Thermo Fisher Scientific Inc., of the United States, was dissolved. When the bismuth nitrate was entirely dissolved, $\text{Fe}(\text{NO}_3)_3 \cdot 9\text{H}_2\text{O}$ and $\text{Sr}(\text{NO}_3)_2$ were gradually

added to the previously mentioned mixed solution. Citric acid was then added, followed by the polymerizing ingredient ethylene glycol, in the order of 1:1:4. The previously mentioned solution turns into a transparent clear sol.

This sol was dried for 24 hours at 80 °C to eliminate most of the water content and create a gel. The metal-citrate complex and the polymer agent transesterified to produce this gel. This gel was then heated to 700 °C and sintered in the air for a period of 4 hours before being cooled to room temperature. The BFO and BSFO nanomaterial was successfully created.

The powder sample was dissolved in 10 wt% of α -terpinol. 10 μ l of this solution was then dropped onto the manufactured sensor substrate 4 pin-TO39 from Umwelt sensor Technik GmbH. The sensor is then given an additional 18 hours of drying time at 80 °C to achieve long-term stability and a smooth surface. Then, the sensor is sintered for two hours at 500 °C to remove any solvent components. A required electronic breadboard is soldered accordingly to make the connections for begin gas sensing measurements. The supporting material characterization were performed and discussed in the doctoral thesis.

5.3 Gas sensing measurement and discussion

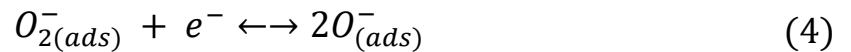
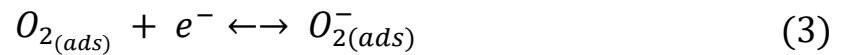
The repeatability of the BSFO sensor shown in Figure 5.2(a) is further evaluated using NO₂ gas with a 100-second injection time and a 2 ppm concentration. It is evident that throughout the course of five cycles, the sensor response remains constant, demonstrating the consistency of all sensor's response and recovery times and their dependability. The inset graphs demonstrate that rapid kinetics is possible and that there is some degree of saturation in this gas injection. Lattice distortion and phase transformation are the obvious causes of this. The increase in carrier concentration and electron mobility causes a subsequent, significantly larger hole accumulation layer at the nanoparticle's surface. Consequently, the performance of the sensing is improved [35].

By adjusting the concentration of the target gas, this sensor may also be tested to determine its lowest detection limit. The sample is analyzed using NO₂ gas, which is delivered into the gas chamber for 150 seconds at concentrations ranging from 200 ppb to 1 ppm. In accordance with our system design, a greater flow rate of 800 sccm was employed to achieve the target gas's low concentrations. The answer from 200 ppb is clearly the lowest, while responses from 400 ppb, 600 ppb, 800 ppb, and 1 ppm are substantially greater and more consistent. This measurement is repeated until 1 ppm in Figure 5.2(b).

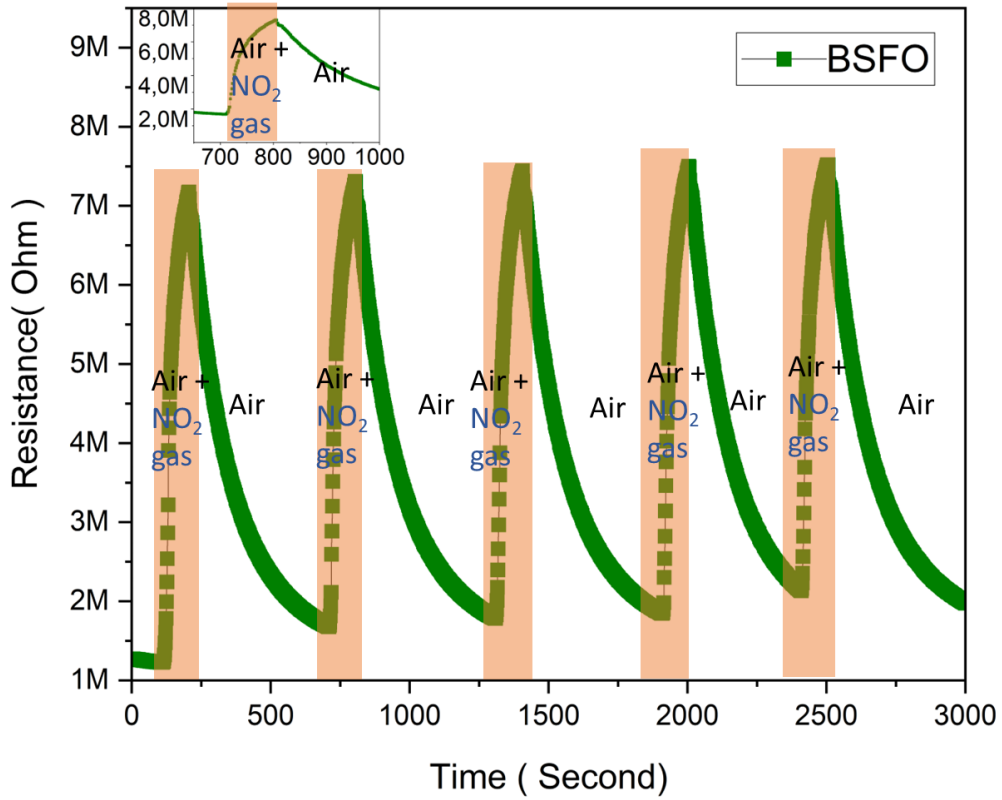
In addition to the impacts of doping, the increased surface area brought on by the nanosized grains also generates additional locations for the NO₂ gas molecules to actively react. To intensify surface reactions, doping also lowers the band gap energy energetically. Figure 5.3(a) shows the computed and displayed T-90 response and T-90 recovery time periods.

As more of the target gas analyte is present in the system, the clearly discernible pattern of the T-90 response time minimizing and the T-90 recovery time increasing is to be expected and explains the viability of the chemical reaction. Figure 5.3(b) displays a calibration curve that was produced using the experimental data. The graph's interference reveals a linear relationship between the sensitivity and logarithm of NO₂ concentration in steady-state circumstances. Showcasing a fairly high R² value of 0.98209, the linear fit equation is Y = 311.64X - 689.94. However, more research is required to assess its long-term stability.

The cross-sensitivity test is the final evaluation. Utilizing the same setup and environmental conditions and the chosen operating temperature of 260 °C. The constructed sensors are evaluated similarly for a transient dynamic response with gas analyte injection for 100 seconds to determine their receptivity to different gases. The sensor response to various gases is shown using a bar graph in Figure 5.4, which shows the concentrations. The BSFO sensor has the greatest response of 4.7 to our analyte gas NO₂ after the sensitivity is computed. This demonstrates further how our target gas is selective in comparison to rival gases in various conditions. Due to system arrangement, the majority of the other gas analytes examined were at greater concentrations, but they nevertheless exhibited close to moderate response sensitivity, with ethanol having the second-largest response at the same concentration, even though it was at a high concentration. The responses to NH₃, CH₄ and CO are minimum. It identifies the sensor's strong specific adsorption capacity for NO₂. Low electron-withdrawing capacity is credited with causing the low gas response. This is most likely caused by the material surface's poor absorption and diffusion. At operational temperature, the reference undoped BFO sensor remained insulating. The gas sensing mechanism for bismuth ferrite has been found to be a p-type sensing behaviour, and as shown above, doping with alters the crystal structure, allowing additional vacancy defects. Oxygen adsorbs on the sensor surface in the air, as shown by reactions (3), (4), and (5).



(a)



(b)

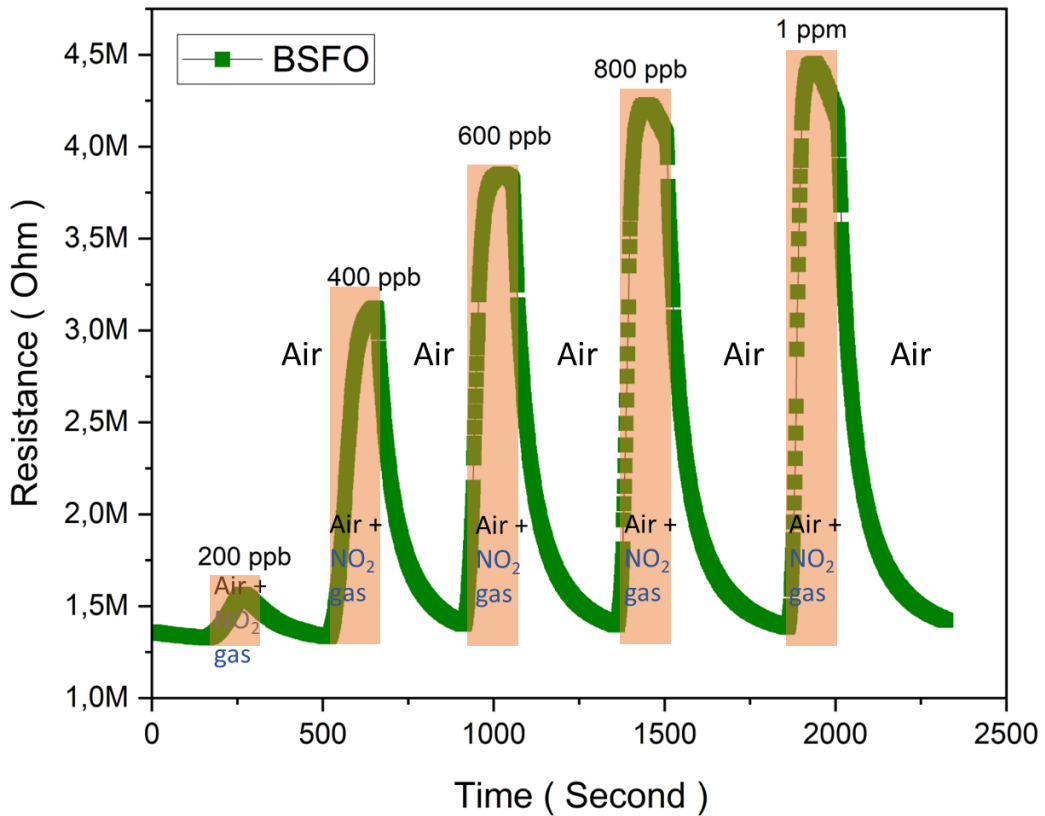


Figure 5.2: Transient response curves of BSFO (a) Repeatability towards 2 ppm of NO_2 at operating temperature; (b) Dynamic sensing characteristics to different concentration of NO_2 at operating temperature [DD1]

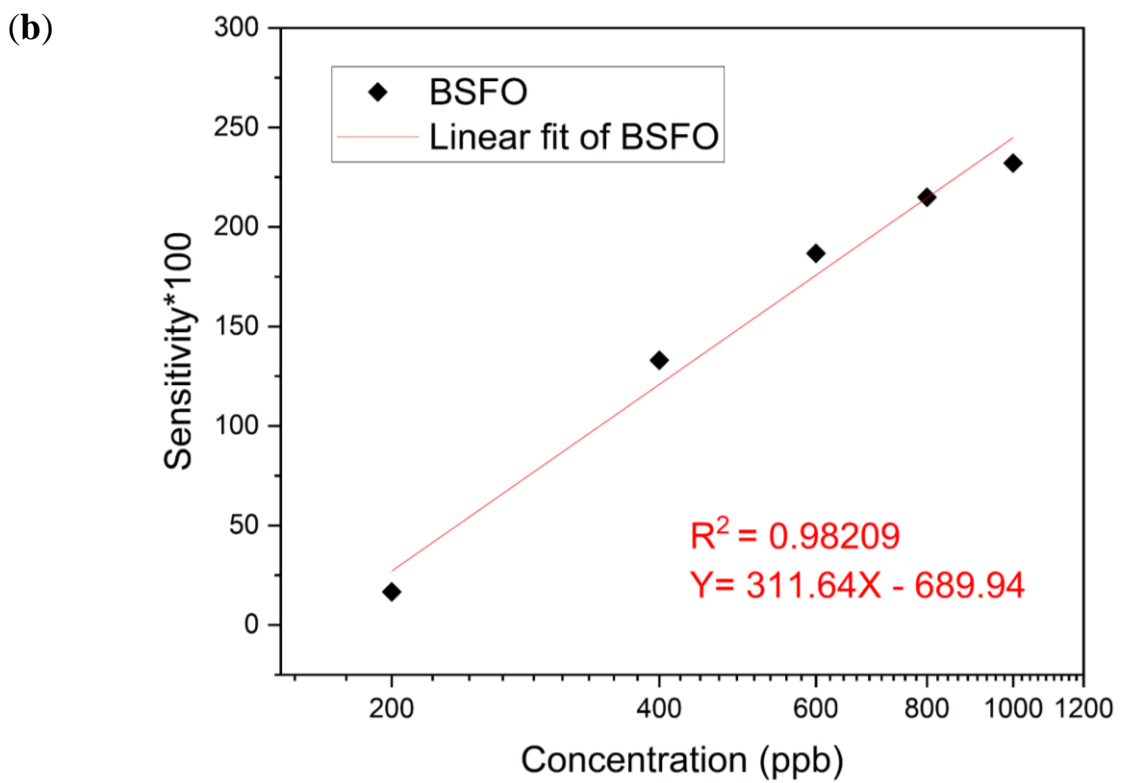
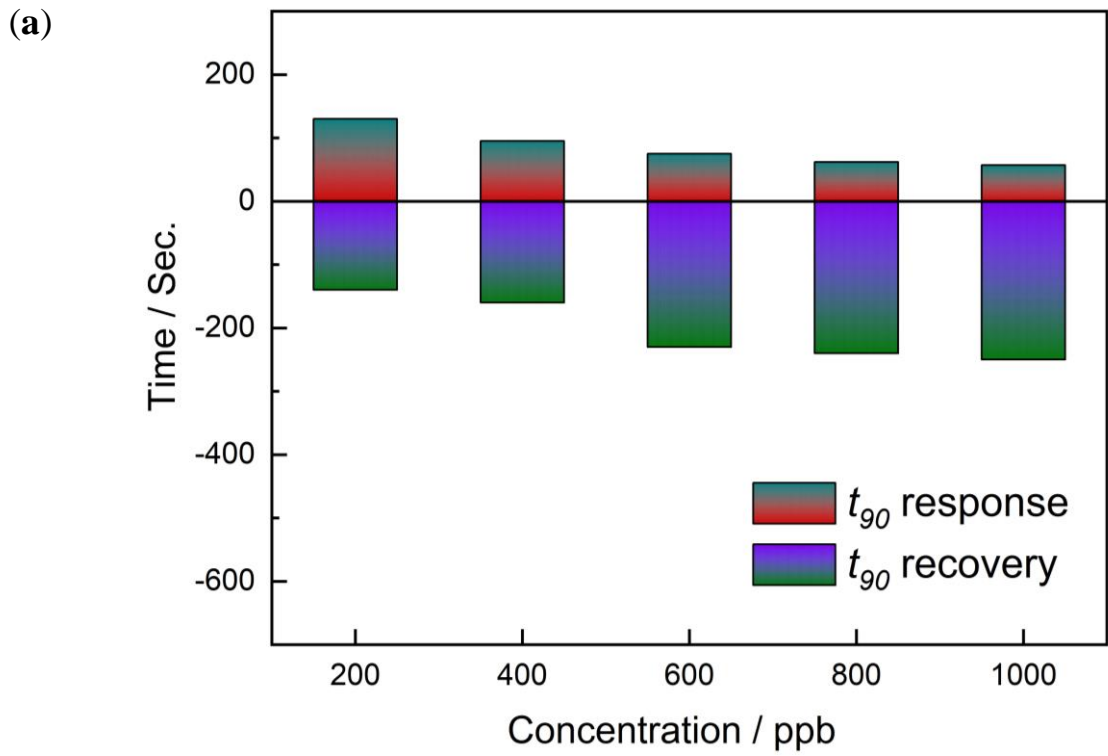


Figure 5.3: (a) Response/recovery dynamics (b) Logarithmic dependency for the BSFO sensor. [DD1]

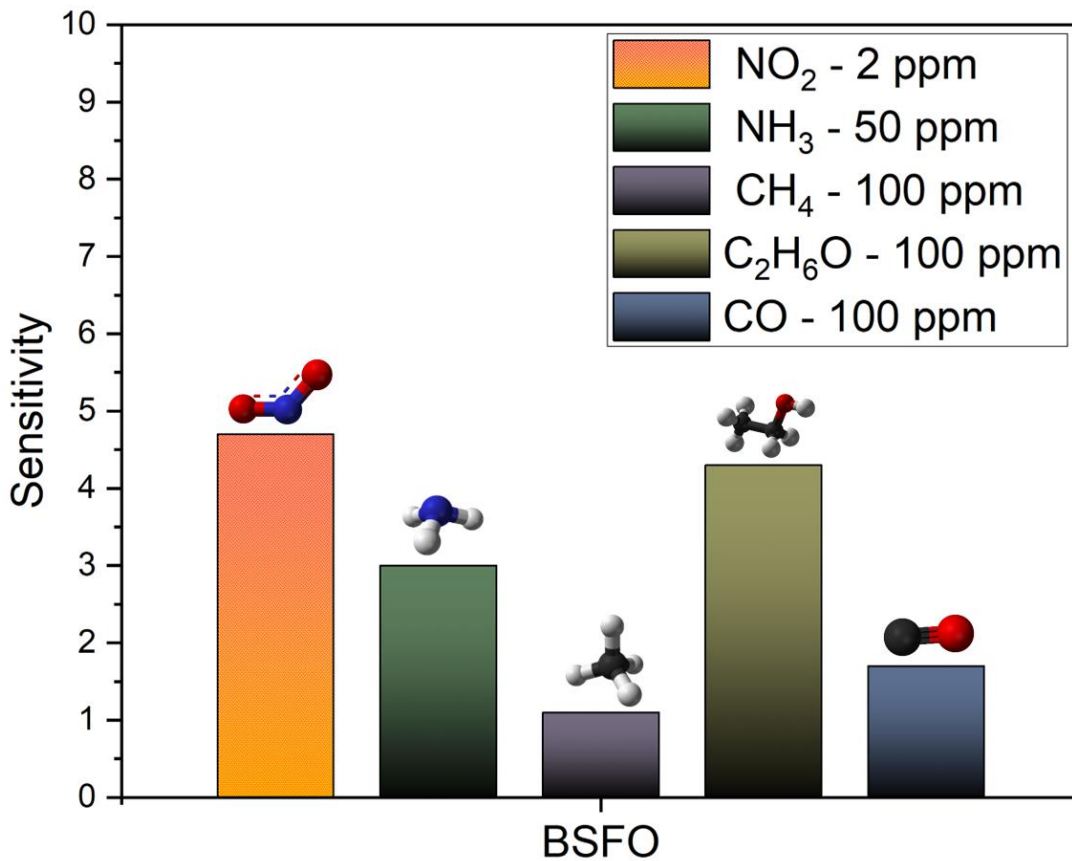


Figure 5.4: Cross sensitivity test for BSFO at operating temperature. [DD1]

This reaction produces an electron-deficient surface because of electron 'trapping' by the adsorbed oxygen during its reduction, raising the electrical resistance of p-type oxides and, as a result, broadening the depletion zone and the degree of band bending [36,37]. The conductive surface in the complex BSFO, as shown in SEM examination, consists of huge micrometre particles and microscopic nano sized crystallites, allowing it to be more porous.

This makes both the surface bulk model and the nano crystals model stated in the research by barsan et al [38] feasible. However, after being oxidized by exposure to low concentrations of NO₂ gas, the resistance increases, indicating merely a change in surface conductivity, indicating an opposing behaviour that could be in contradiction with the material's bulk conductivity. The surface adsorbed atomic oxygen species combines with the high affinity NO₂ gas, lowering the electron concentration near the surface and causing recombination with the holes, causing the resistance to rise.

The strontium dopant acts as a catalyst, lowering the work function required for the reversible process and allowing for more binding sites. This explains the ability to detect low concentrations. Thus, the sensing performance has substantially increased in comparison to pure bismuth ferrite due to the synergistic effect of both bismuth ferrite and strontium dopant.

6. Chromium vanadate Studies

6.1 Gas sensing system

Gas sensing measurements are made using the same setup and methodology as described previously. The sensitivity/relative response to the change in gas concentration in this part of the work was calculated using the formula below.

$$R\% = \frac{R_a - R_g}{R_a} * 100 \quad (6)$$

$$R\% = \frac{R_g - R_a}{R_a} * 100 \quad (7)$$

Equation (1) applies to reducing gases, while equation (2) applies to oxidizing gases. R_g and R_a represent the sensor's resistance in the presence of analyte and the sensor's resistance in synthetic air, respectively.

6.2 Material preparation

CrVO_4 was synthesized by a slightly modified version of a co-precipitation method as described here[39]. 1 mM chromium nitrate was dissolved in 50 mL of deionized (DI) water. In a similar manner, 50 mL of warm DI water was employed to dissolve 1 mM of ammonium metavanadate. Subsequently, the solutions were combined and agitated for an additional duration of two hours. Following this, a solid precipitate was generated and cautiously gathered. The ensuing precipitate was subsequently subjected to three rounds of washing with ethanol and DI water. It was then placed for calcination within a tube furnace for a duration of two hours at a temperature of 600 °C, under the presence of an argon atmosphere. Consequently, the desired product, CrVO_4 , was obtained.

The same methodology is used to prepare the sensor from the previous research work. Similarly, Three sensors are prepared using the same techniques. The supporting material characterization were performed and discussed in the doctoral thesis.

6.3 Gas sensing measurement and discussion

The sensor is tested for repeatability as depicted in the graph in Figure 6.1. It shows that the CrVO_4 sensor response able to give consistent response over three successive cycles of gas infusion for a total time span of 1600 seconds, or nearly 27 minutes. It shows a stable reaction, with an expected T-90 response and T-90 recovery time of 83 seconds and 325 seconds towards 100 seconds of NH_3 gas infusion, respectively. This may be due to the more cleaved lattice structure, which allows for more oxygen vacancies, as well as the nano size effect [40,41].

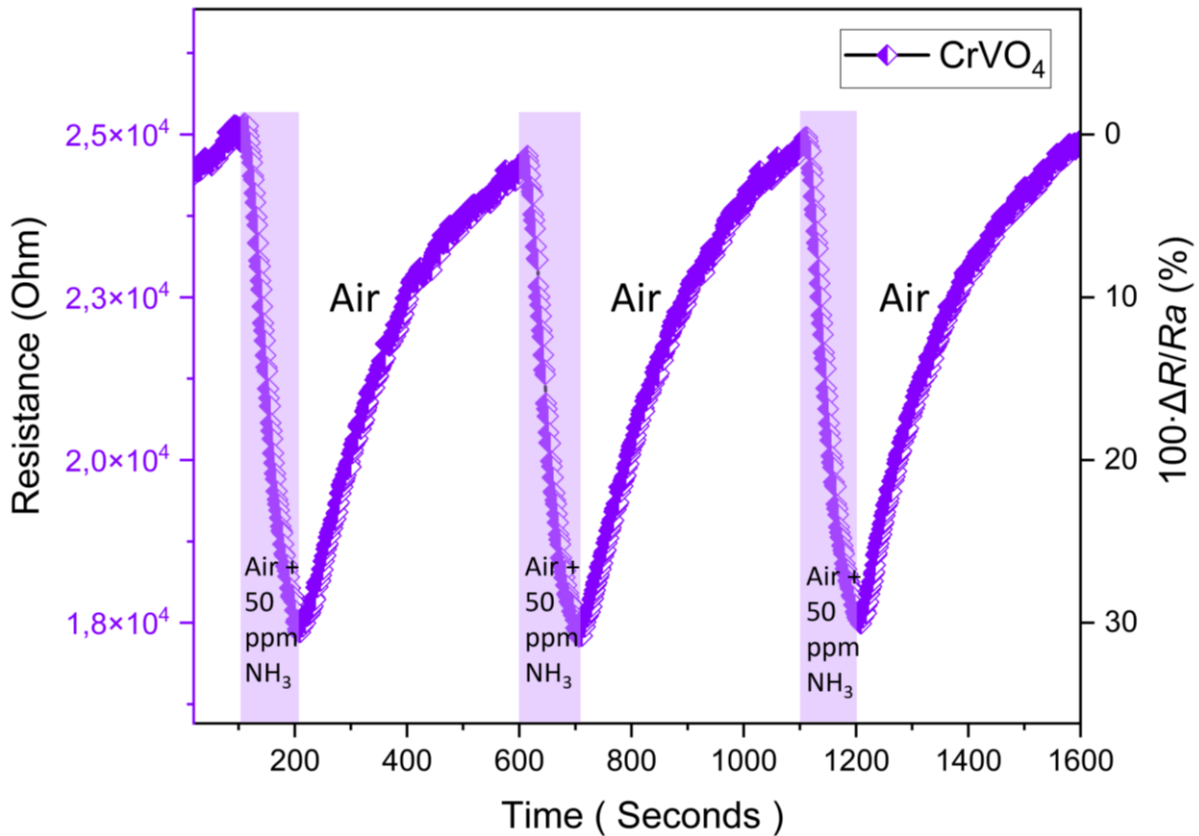


Figure 6.1: Transient response curve of repeatability towards NH_3 [DD2]

Altering the concentration of the target gas is another test to determine the CrVO_4 sensor's LOD (Limit of detection). It is analysed using NH_3 gas, which is introduced into the gas chamber from 10 ppm to 100 ppm for 100 seconds. As per our system design, a higher flow rate of 800 sccm was used to reach low concentrations of target gas. It must be noted that the change in flow rate of the target gas has also changed the base line resistance value. However, these changes does not affect our response calculation. In the Figure 6.2 the sensor exhibited an appropriate response to different concentrations sequentially towards our target gas.

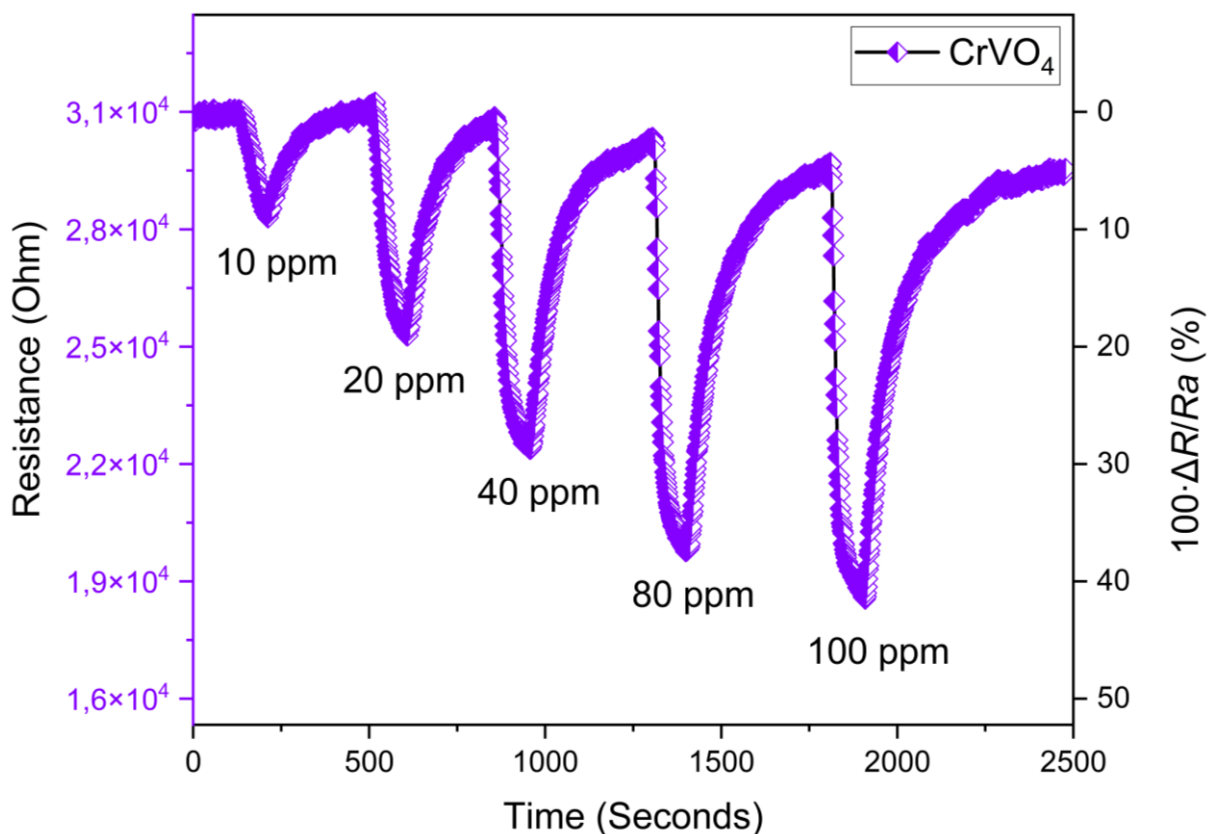


Figure 6.2: Dynamic sensing characteristics to different concentration of NH_3 at operating temperature [DD2]

The response to the lowest gas concentration is further analysed and it can be seen in Figure 6.3. Therefore, for a 10 ppm gas response, it takes more than 13 times 3σ levels to reach the detection peak of our least recorded response if the average noise is fixed at σ . This shows unambiguously that baseline noise has no effect on the response. As generally accepted minimum value of the signal-to-noise ratio ($n = 3\sigma$). This permits for the conclusion that its real LOD is probably much lower than the one detected, as the experimental value in the above measurement is limited by the given flow controllers and the gas sensing system fit with gas cylinders of certain concentrations. From the signal-to-noise ratio graph, it can be estimated that ca 0.7 ppm of gas analyte (given that the signal at 10 ppm is equivalent to roughly 39σ) is the value point from which a clear difference is seen from baseline noise. This allows us to have a similar LOD value as reported [42], albeit without any noble elements.

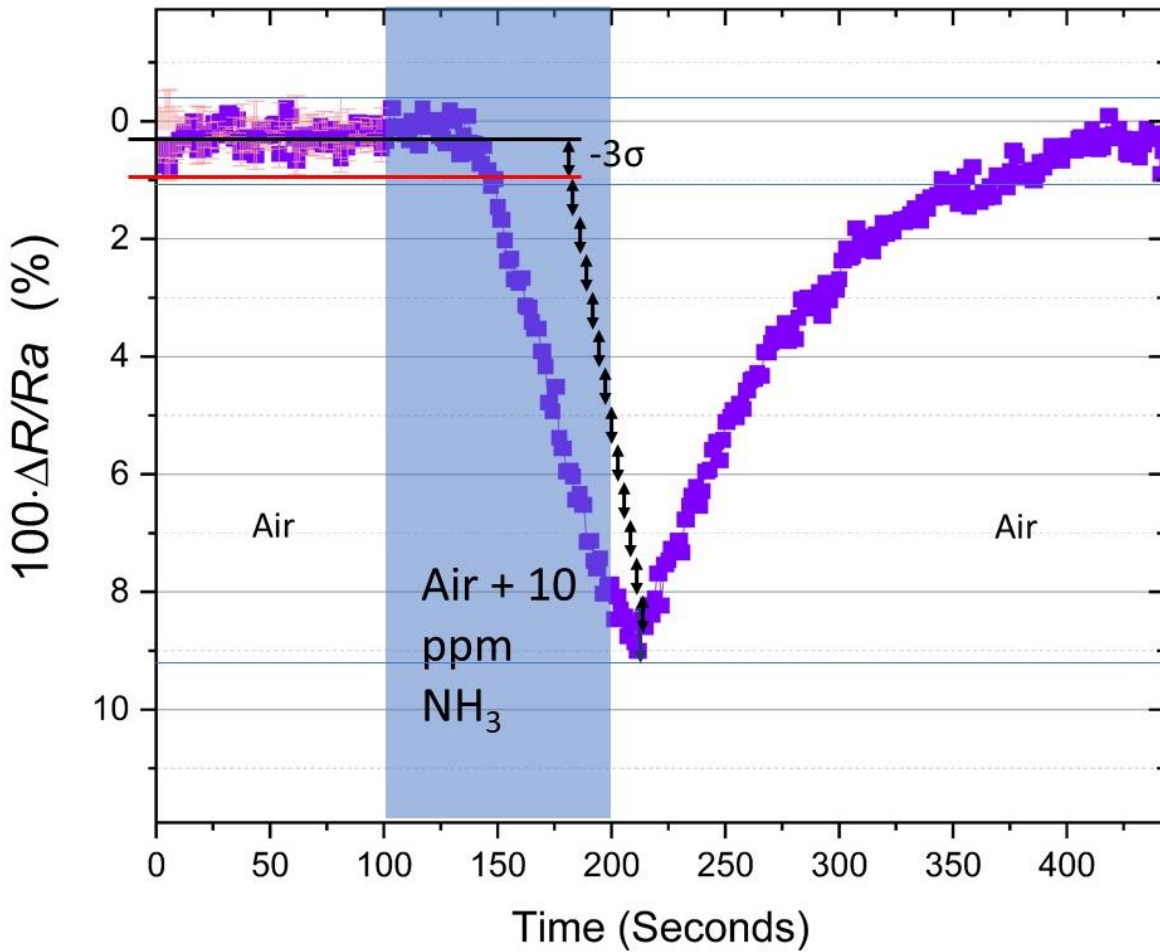


Figure 6.3: LOD analysis from optimal sensing curve of CrVO_4 sensor [DD2].

The T-90 response and T-90 recovery is calculated and plotted in the Figure 6.4(a). It shows the expected trend of faster T-90 response times and slower T-90 recovery times as gas concentration increases in ppm due to reaction feasibility. Figure 6.4 (b) shows a calibration curve that was produced using the experimental data. The graph's interference reveals a linear relationship between the sensitivity and the logarithmic concentration of NH_3 gas in constant conditions. With a relatively high R^2 value of 0.99835, the linear fit equation for our response values show high correlation along $Y = 30.6X + 8.53$. Essentially, the sensor response, certainly within the studied range of experimental conditions, exhibits logarithmic growth with increasing concentration. An Asymptotic exponential growth model will be more fitting if sensor saturation is presumed for higher concentrations. Although, the logarithmic growth model provides a mathematical description that is appropriate for the range under investigation.

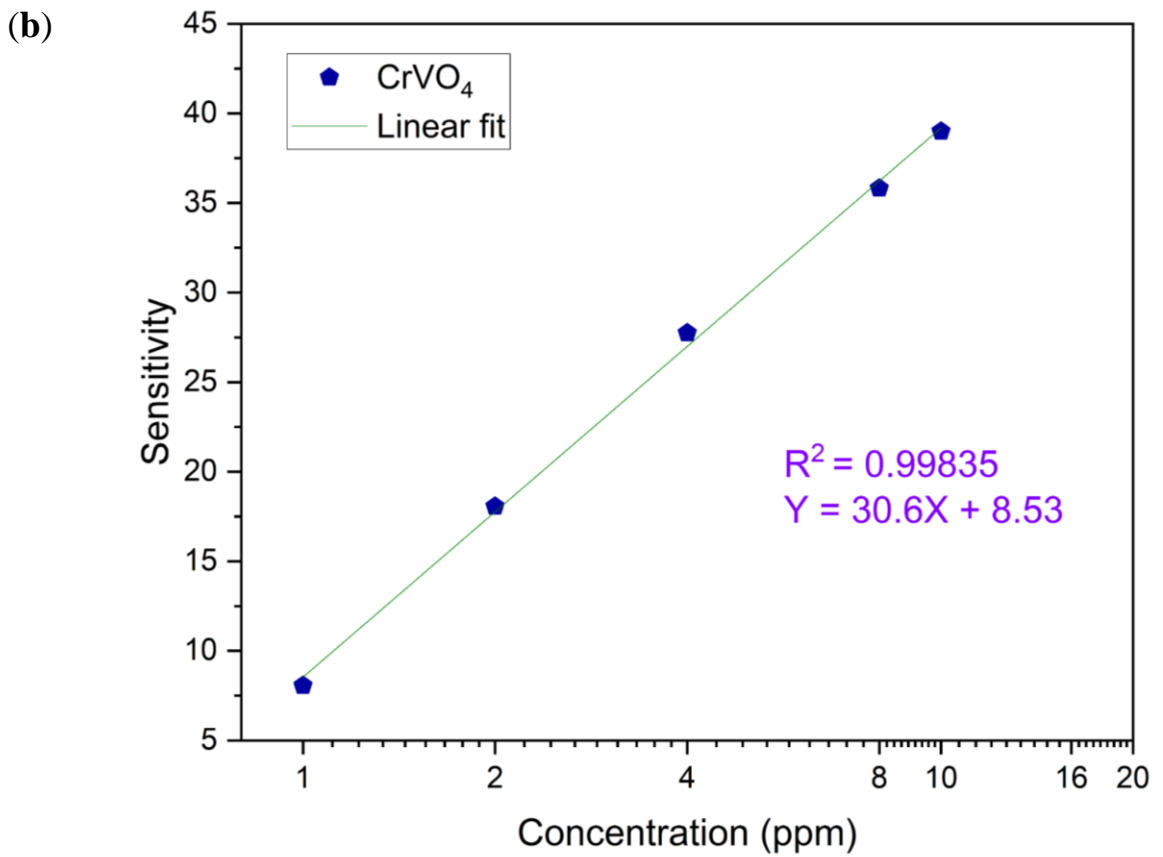
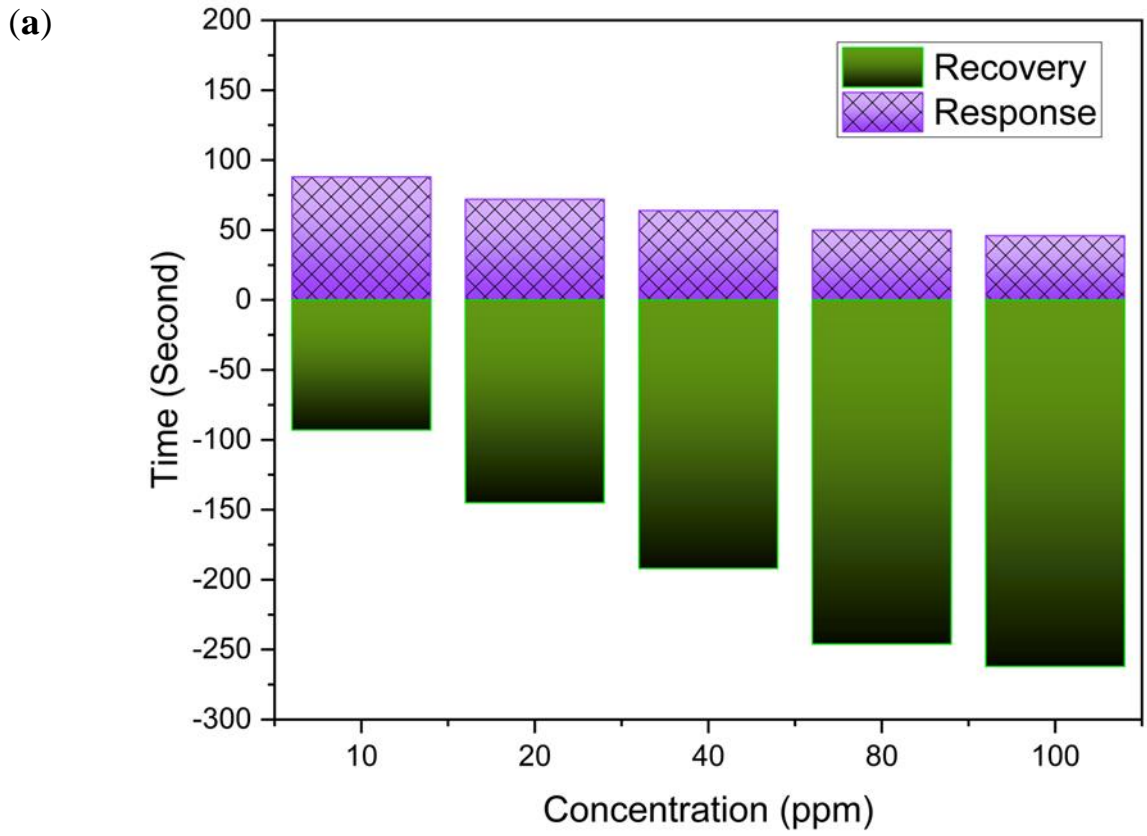


Figure 6.4: (a) Response/recovery dynamics (b) Logarithmic dependency for the CrVO_4 sensor [DD2]

The cross-sensitivity test is the next assessment shown in Figure 6.5. Utilising the given setup and environmental conditions and the chosen operating temperature of 330 °C for best performance towards our target gas. The constructed CrVO₄ sensor is evaluated similarly for a transient dynamic response with gas analyte injection for 100 seconds to determine their sensitivity to different gases. The concentrations are NH₃ at 50 ppm, C₂H₆O at 100 ppm, CH₄ at 100 ppm, NO₂ at 100 ppm and CO at 100 ppm. It is very clearly seen that our sensor is selective to our target gas while the response to other gases shows minimum response with 17 percent at best. A reduced ability to donate electrons and poor reaction kinetics is attributed to the comparatively lower response to the other gases tested.

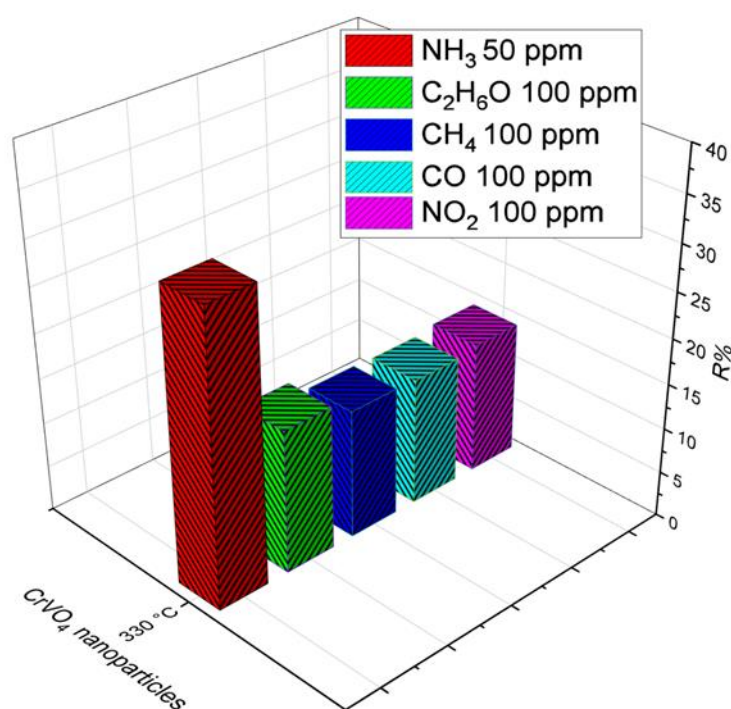
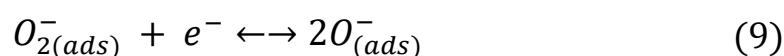
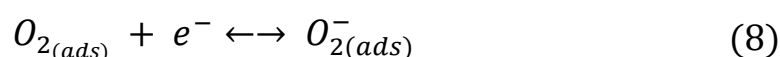


Figure 6.5: Cross sensitivity testing for CrVO₄ sensor.

In this current work, possible gas sensing mechanism is explained for sensing material CrVO₄. It is a known insulator in room temperature but after 150 °C, it shows to be weakly conductive in our sensor substrate. At the operating temperature of 330 °C, it is possible that the following reaction happens with oxygen and the majority species adsorbed on the surface are O⁻ atomic oxygen cause energy band bending. The equation is depicted in equations below:-



CrVO₄ is said to have p-type electrical conductivity, as reported by T.gro et al [43]. Because of the large number of unoccupied spaces and severely deformed polyhedral units in the lattice of CrVO₄-type formations, the dielectric and conduction processes may have distinct influence in addition to the participation of electrons due to valence fluctuation because of the significant number of empty spaces and significantly distorted polyhedral units in the CrVO₄ type lattice structures [44,45].

The operating principle of sensing layer, as explained by Barsan et al,[46]. illustrates that it can be impacted by a variety of conduction methods. Our material's surface is also found to be quite complex with perhaps poorly sintered large grains, narrow necks, and small grains. The surface influence and energy band bending identified in the research appear to have the most influence on this mechanism.

According to literature [46], When the material is used in air and at higher temperatures, active oxygen species that cover its surface affect the concentration of holes. O⁻ ions are the predominant oxygen species adsorbed on the surface at the operating temperature of 330 °C, which results in energy band bending. [47]. It can be presumed that the NH₃ gas molecules on interaction with the chemisorbed O⁻ react and release electrons back into the conduction band. This can be seen as decrease in the overall resistance allowing more hole mobility. Therefore, the reducing gas reacts with the partial consumption of preabsorbed oxygen ions on the surface. In this process of recovery, this reaction of majority O⁻ carriers after cleaving from the gas molecules absorb on the surface again , thereby increasing the baseline resistance.

The changes in concentration of charge carriers on the material surface induce modifications in the work function (ϕ), electron affinity (χ) and the band bending (qV) of the active sensing material. These contributing factors alter the electronic property and this modification of band bending ($q\Delta V$) can be determined from the sensing efficiency [48] and using the equation below.

$$q\Delta V = -2k_B T \ln\left(\frac{R_G}{R_A}\right) \quad (10)$$

where T is the temperature, k_B is the Boltzmann constant, R_A is the sensor resistance in air and R_G is the sensor resistance in gas. The Figure 6.6 illustrates the plot with the value of $q\Delta V$ in relation to the sensor response in different concentrations of NH₃ gas. As saturation at high analyte concentration approaches, the band bending displays a logarithmic growth curve or maybe an asymptotic exponential growth, which is to be expected. It is in line with the calibration dependency as shown in the Figure 6.4(b).

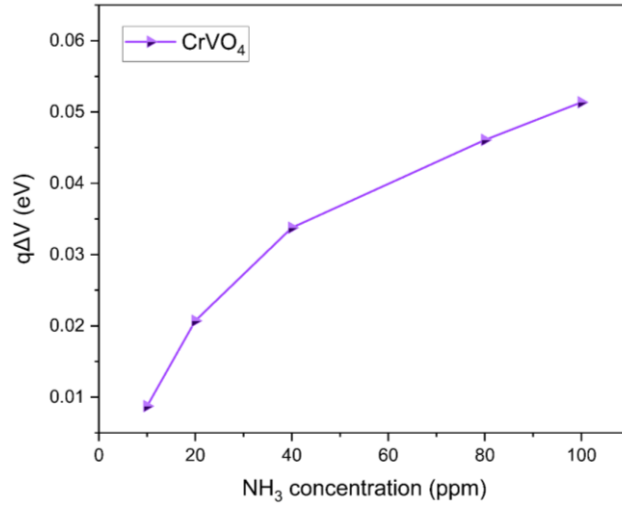


Figure 6.6: The change in induced band bending ($q\Delta V$) over NH_3 gas concentration [DD2].

As a result of variations in the charge density in the depletion layer on the outer surface layer of the material grains and resulting drop in band bending ($q\Delta V$) surface reactions and mutual interactions of adsorbed species affect surface conductivity. As seen in Figure 6.7, a positive value of $q\Delta V$ denotes a reduction in the band bending qV and a shift in the Fermi level (E_F) towards higher values. Based on an analogy with the literature pertaining to our specific operating temperature circumstances, gas compositions and concentrations, and likely surface effects, the sensing principle has been schematized. effects [49–52]. $E_{v, bulk}$ and $E_{c, bulk}$ indicate the conduction and valence band edge energy levels in bulk, respectively. E_F stands for Fermi level, E_g indicates the forbidden gap energy and E_{vac} indicates the vacuum level. The induced band bending is determined by $q\Delta V$. and lastly, the band bending is indicated as qV .

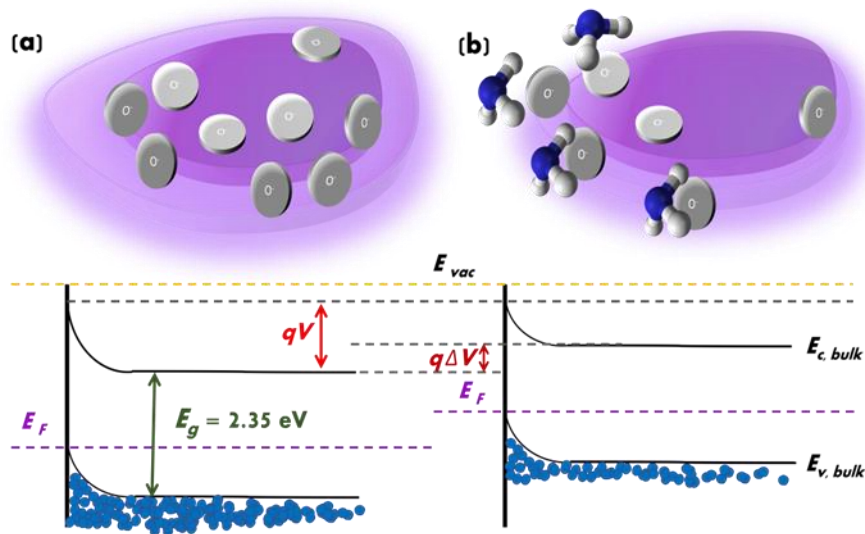


Figure 6.7: Band bending (a) in the presence of atomic oxygen species (b) in the presence of ammonia towards our CrVO_4 sensor [DD2].

7. Summary of results and outlook

The results, conclusions, and findings presented in this thesis can be divided into three parts following the subdivision of the main goal, labelled Goal A, i.e., zinc oxide sensing studies, bismuth ferrite sensing studies, and chromium vanadate sensing studies. The achievements in material preparation and synthesis according to the second goal, labelled Goal B, are mentioned wherever appropriate. Future challenges and remaining question have been identified as well.

Zinc oxide sensing studies

In the first part of this dissertation, ZnO nanorods are grown with different parameters for optimal growth and a prototype sensing device is fabricated. The preparation of these nanostructures and the control of their growth is successful in terms of their variable morphology.

Next, a simple and new method for preparation of gas sensors for organic vapours such as ethanol was developed by using material inkjet printing using both commercial as well as fabricated inks and substrates for developing a sensing device. In the field of methodology, a testing apparatus for response measurements of prepared sensors was developed. However, the relative response is still low and this research requires more experimentation and optimization to surpass current market level sensitivity and make it possible in room temperature without the necessity to heat the sensor up to 200°C. High temperature operation is a contemporary must for this type of sensors and limits significantly the current application of this sensor.

Although this part of the work succeeded only partially in the main goal, it delivered interesting results in the field of the secondary goal and stimulated other works using hydrothermal preparation of zinc oxide nanoforests.

Employment of an integrated UV source into the sensor device is envisaged for further work, yet this idea still fights many practical problems. The UV shall deliver photons of sufficient energy to replace the role of high temperature in the surface sorption/desorption and molecule dissociation equilibria. Additionally, the next step of proposed research is surface modification of prepared nanostructures by thin polymer coatings or decorations to impart selectivity to the prepared sensors. Then, the enhanced selectivity effect shall be based on specific interaction of the vapour molecules with the polymer.

To further improve this work, a puzzling scientific challenge is to address the sensing mechanism in prepared sensors, since it seems neither of the most widely accepted standard models works well. A comparative study of sensing behaviour in air and in pure nitrogen atmosphere should decipher this issue.

Bismuth ferrite sensing studies

In the second part of the research work, bismuth ferrite sensors and Sr-doped bismuth ferrite nanostructures were synthesized by sol-gel using various precursors at 700 °C. The XRD spectra have identified a single crystal structure of both bismuth ferrite and Sr doped bismuth ferrite. Surface morphology and particle size of irregular plates between 30 nm and 100 nm. It is very clear that the doping has further reduced the overall size of the nanoparticles.

This composition for both BFO and BSFO in EDX corresponds to the literature. The XPS spectra confirm the existence of predicted BFO components and the dopant in BSFO. The nanostructures when used as gas sensing materials to construct sensors for NO₂ showed the highest relative response of 520 % in our testing. The repeatability and gas concentration variation tests are shown with a linear fitting along the relative response, where the limit of detection for BSFO is 200 ppb.

The response and recovery times can be further improved on structural modification into nanofibers etc. These results confirm that the Sr-doped bismuth ferrite enable a lower working temperature, higher response and are promising sensing materials for the development of low-cost, easily fabricated, stable, selective and high performance NO₂ gas sensors. Interference studies and testing in ambient air can add more value as it shows a more realistic behaviour of the sensor in it's proposed applicative situation. More research is needed to understand the stability of the sensor over long-term usage, and it can be further improved with other techniques.

To further improve this work, to improve the comprehension of the mechanism involved in this sensor, we must use more comprehensive equipment such as Temperature Programmed Desorption-Mass Spectrometry (TPD-MS) etc.

Chromium vanadate sensing studies

In the third part of this dissertation, chromium orthovanadate nanostructures were synthesized by co-precipitate method. The XRD spectra have identified as a monocystal structure of mainly a monoclinic system belonging to the space group C2/m. Surface morphology and particle size are in correlation with literature description. Particle size of around 30 nm and these nanoplatelets surface shape overlap aggregating in bigger particles.

The as-prepared nanostructures when used as gas sensing materials to construct sensors for NH₃ gas showed the highest relative response of 32 percent to the baseline in our cross testing. A linear fitting along relative response is used to display the variation in gas concentration, where the limit of detection for CrVO₄ is 10 ppm with a range of detection up to 100 ppm. The estimated value above can be seen to be circa 0.7 ppm and it is ideal to do more gas sensing investigation, such as long-term repeatability. This is slightly better than the best contemporary reported LOD value of 1 ppm, but the chromium vanadate sensor works without any noble

elements in its structure. The response and recovery times can be further improved on structural modification.

These results confirm that the CrVO_4 nanomaterial offer a selective gas sensor which is also low-cost, easily fabricated, and offers stable performance towards NH_3 gas. It showed notable sensitivity, linearity of distribution, and selectivity, indicating its potential use in ppm concentration ammonia gas detection. Interference experiments and testing in ambient air possess the potential to enhance the significance of a sensor's potential by portraying a more authentic behaviour within its intended operational environment. Further investigations are warranted to comprehend the sensor's durability throughout extended periods of usage, and to explore the possibility of enhancing its performance through additional methodologies.

Furthermore, this work contributed to the understanding of the sensing process; nevertheless, additional and more comprehensive instrumented research including Temperature Programmed Desorption-Mass Spectrometry (TPD-MS) would be required to completely elucidate the mechanisms.

8. Contribution to science and practice

The work contributes to the general knowledge as well as to the technology (including laboratory techniques) accordingly to the aim of this thesis:

Zinc oxide sensing studies

- A simple and new method for preparation of electrode patterns on various substrates, including flexible films was developed by using material inkjet printer.
- Nanoparticle ink was prepared, characterized, and used to grow nanorods with variations in their aspect ratio on different substrates.
- A testing apparatus for gas response measurements of prepared sensors was developed and installed at the Centre of Polymer systems.

Bismuth ferrite sensing studies

- A simple method is modified for the preparation of a single crystal structure of multiferroic bismuth ferrite and strontium doped bismuth ferrite.
- The bismuth ferrite nanomaterials were characterized to give an in-depth comprehension of the material properties.
- A testing apparatus for response measurements of fabricated sensors was developed and installed at the Inorganic Chemistry laboratory in Cologne.
- The sensors developed showed unique gas sensing properties towards our target gas NO_2 with the lowest recorded LOD response values among our collaborative partner labs yet.

Chromium vanadate sensing studies

- A simple method is modified for the preparation of a single crystal structure of chromium vanadate.
- The chromium vanadate nanomaterials were characterized to give an in-depth comprehension of the material properties.
- The sensors developed showed unique gas sensing properties towards our target gas NH_3 and is also the first reported prototype chemo sensing device of this nanomaterial yet.
- The limit of detection (LOD) of this pioneering sensor, prepared from chromium vanadate, is at least comparable to or better than that of any currently reported sensor, even without the need for noble metals which is essential for the functionality of top competing reported sensor.

References

Author articles

[DD1] Dmonte, David John; Bhardwaj, Aman; Wilhelm, Michael; Fischer, Thomas; Kuřitka, Ivo; Mathur, Sanjay; Sub PPM Detection of NO₂ Using Strontium Doped Bismuth Ferrite Nanostructures, *Micromachines*, 14, 3, 644, 2023, MDPI

[DD2] Dmonte, David John; Bhardwaj, Aman; Kavraz, Pelin; Slobodian, Rostislav; Antos, Jan; Sisman, Orhan; Galusek, Dusan; Fischer, Thomas; Mathur, Sanjay; Kuritka, Ivo; Detection of NH₃ gas using CrVO₄ nanoparticles, *Sensors and Actuators B: Chemical*, 135380, 2024, Elsevier

Other References

- [1] Y. Liu, K. He, G. Chen, W.R. Leow, X. Chen, Nature-Inspired Structural Materials for Flexible Electronic Devices, *Chem Rev* 117 (2017) 12893–12941. <https://doi.org/10.1021/ACS.CHEMREV.7B00291>.
- [2] Z. Zhu, D.W.H. Ng, H.S. Park, M.C. McAlpine, 3D-printed multifunctional materials enabled by artificial-intelligence-assisted fabrication technologies, *Nat Rev Mater* 6 (2020) 27–47. <https://doi.org/10.1038/S41578-020-00235-2>.
- [3] I. Rahwan, M. Cebrian, N. Obradovich, J. Bongard, J.F. Bonnefon, C. Breazeal, J.W. Crandall, N.A. Christakis, I.D. Couzin, M.O. Jackson, N.R. Jennings, E. Kamar, I.M. Kloumann, H. Larochelle, D. Lazer, R. McElreath, A. Mislove, D.C. Parkes, A. ‘Sandy’ Pentland, M.E. Roberts, A. Shariff, J.B. Tenenbaum, M. Wellman, Machine behaviour, *Nature* 568 (2019) 477–486. <https://doi.org/10.1038/S41586-019-1138-Y>.
- [4] A.J. Perez, S. Zeadally, Recent Advances in Wearable Sensing Technologies, *Sensors (Basel)* 21 (2021) 6828. <https://doi.org/10.3390/S21206828>.
- [5] Z. Lou, L. Wang, G. Shen, Z. Lou, G.Z. Shen, L.L. Wang, Recent Advances in Smart Wearable Sensing Systems, *Adv Mater Technol* 3 (2018) 1800444. <https://doi.org/10.1002/ADMT.201800444>.
- [6] B. Mazzolai, C. Laschi, A vision for future bioinspired and biohybrid robots, *Sci Robot* 5 (2020). <https://doi.org/10.1126/SCIROBOTICS.ABA6893>.
- [7] X. Yu, H. Cheng, M. Zhang, Y. Zhao, L. Qu, G. Shi, Graphene-based smart materials, *Nature Reviews Materials* 2017 2:9 2 (2017) 1–13. <https://doi.org/10.1038/natrevmats.2017.46>.
- [8] X. Qiu, S. Hu, “Smart” Materials Based on Cellulose: A Review of the Preparations, Properties, and Applications, *Materials (Basel)* 6 (2013) 738–781. <https://doi.org/10.3390/MA6030738>.
- [9] M. Yoshida, J. Lahann, Smart nanomaterials, *ACS Nano* 2 (2008) 1101–1107. <https://doi.org/10.1021/NN800332G>.

- [10] M. Stoppa, A. Chiolerio, Wearable Electronics and Smart Textiles: A Critical Review, *Sensors* 2014, Vol. 14, Pages 11957-11992 14 (2014) 11957–11992. <https://doi.org/10.3390/S140711957>.
- [11] D. Hassabis, D. Kumaran, C. Summerfield, M. Botvinick, Neuroscience-Inspired Artificial Intelligence, *Neuron* 95 (2017) 245–258. <https://doi.org/10.1016/J.NEURON.2017.06.011>.
- [12] J.H. Koo, D.C. Kim, H.J. Shim, T.H. Kim, D.H. Kim, Flexible and Stretchable Smart Display: Materials, Fabrication, Device Design, and System Integration, *Adv Funct Mater* 28 (2018) 1801834. <https://doi.org/10.1002/ADFM.201801834>.
- [13] G.Z. Yang, P. Fischer, B. Nelson, New materials for next-generation robots, *Sci Robot* 2 (2017). <https://doi.org/10.1126/SCIROBOTICS.AAP9294>.
- [14] R. Karunakaran, S. Ortgies, A. Tamayol, F. Bobaru, M.P. Sealy, Additive manufacturing of magnesium alloys, *Bioact Mater* 5 (2020) 44–54. <https://doi.org/10.1016/J.BIOACTMAT.2019.12.004>.
- [15] V. Chabot, D. Higgins, A. Yu, X. Xiao, Z. Chen, J. Zhang, A review of graphene and graphene oxide sponge: material synthesis and applications to energy and the environment, *Energy Environ Sci* 7 (2014) 1564–1596. <https://doi.org/10.1039/C3EE43385D>.
- [16] R. Bogue, Terrorism and military actions pose the ultimate challenge to gas sensing, *Sensor Review* 31 (2011) 6–12. <https://doi.org/10.1108/02602281111099026/FULL/PDF>.
- [17] E.A. Baldwin, J. Bai, A. Plotto, S. Dea, Electronic Noses and Tongues: Applications for the Food and Pharmaceutical Industries, *Sensors* 2011, Vol. 11, Pages 4744-4766 11 (2011) 4744–4766. <https://doi.org/10.3390/S110504744>.
- [18] X.Q. Jiang, X.D. Mei, D. Feng, Air pollution and chronic airway diseases: what should people know and do?, *J Thorac Dis* 8 (2016) E31–E40. <https://doi.org/10.3978/J.ISSN.2072-1439.2015.11.50>.
- [19] M.E. Franke, T.J. Koplin, U. Simon, Metal and metal oxide nanoparticles in chemiresistors: does the nanoscale matter?, *Small* 2 (2006) 36–50. <https://doi.org/10.1002/SMLL.200500261>.
- [20] S. Yang, C. Jiang, S. huai Wei, Gas sensing in 2D materials, *Appl Phys Rev* 4 (2017). <https://doi.org/10.1063/1.4983310/279723>.
- [21] K.J. Choi, H.W. Jang, One-Dimensional Oxide Nanostructures as Gas-Sensing Materials: Review and Issues, *Sensors (Basel)* 10 (2010) 4083–4099. <https://doi.org/10.3390/s100404083>.
- [22] G. Jiménez-Cadena, J. Riu, F.X. Rius, Gas sensors based on nanostructured materials, *Analyst* 132 (2007) 1083–1099. <https://doi.org/10.1039/B704562J>.

- [23] J. Li, Y. Lu, Q. Ye, M. Cinke, J. Han, M. Meyyappan, Carbon nanotube sensors for gas and organic vapor detection, *Nano Lett* 3 (2003) 929–933. <https://doi.org/10.1021/NL034220X/ASSET/IMAGES/LARGE/NL034220X.F00005.JPEG>.
- [24] M. Meyyappan, Carbon Nanotube-Based Chemical Sensors, *Small* 12 (2016) 2118–2129. <https://doi.org/10.1002/SMLL.201502555>.
- [25] H. Ji, W. Zeng, Y. Li, Gas sensing mechanisms of metal oxide semiconductors: a focus review, *Nanoscale* 11 (2019) 22664–22684. <https://doi.org/10.1039/C9NR07699A>.
- [26] S.H. Lee, K.Y. Shin, J.Y. Hwang, K.T. Kang, H.S. Kang, Silver inkjet printing with control of surface energy and substrate temperature, *Journal of Micromechanics and Microengineering* 18 (2008) 075014. <https://doi.org/10.1088/0960-1317/18/7/075014>.
- [27] Y.I. Lee, Y.S. Goo, K.J. Lee, Y.G. Hwang, Y. Byun, H.J. Park, D.Y. Park, N. V. Myung, Y.H. Choa, Effect of UV/ozone treatment on interactions between ink-jet printed Cu patterns and polyimide substrates, *Thin Solid Films* 519 (2011) 6853–6857. <https://doi.org/10.1016/J.TSF.2011.04.050>.
- [28] A.C. Guler, J. Antos, M. Masar, M. Urbanek, M. Machovsky, I. Kuritka, Comprehensive evaluation of photoelectrochemical performance dependence on geometric features of ZnO nanorod electrodes, *Nanoscale Adv* 5 (2023) 3091–3103. <https://doi.org/10.1039/D3NA00089C>.
- [29] B. Derby, Inkjet Printing of Functional and Structural Materials: Fluid Property Requirements, Feature Stability, and Resolution, <https://doi.org/10.1146/Annurev-Matsci-070909-104502> 40 (2010) 395–414. <https://doi.org/10.1146/ANNUREV-MATSCI-070909-104502>.
- [30] L.G. Toy, K. Nagai, B.D. Freeman, I. Pinnau, Z. He, T. Masuda, M. Teraguchi, Y.P. Yampolskii, Pure-gas and vapor permeation and sorption properties of poly[1-phenyl-2-[p-(trimethylsilyl)phenyl]acetylene] (PTMSDPA), *Macromolecules* 33 (2000) 2516–2524. <https://doi.org/10.1021/MA991566E/ASSET/IMAGES/MEDIUM/MA991566EE00011.GIF>.
- [31] A. Queraltó, D. Graf, R. Frohnhoven, T. Fischer, H. Vanrompay, S. Bals, A. Bartasyte, S. Mathur, LaFeO₃ Nanofibers for High Detection of Sulfur-Containing Gases, *ACS Sustain Chem Eng* 7 (2019) 6023–6032. https://doi.org/10.1021/ACSSUSCHEMENG.8B06132/SUPPL_FILE/SC8B06132_SI_001.PDF.
- [32] A. Raauf, D. Graf, Y. Gönüllü, P.K. Sekhar, M. Frank, S. Mathur, Synergistic Acceptor-Donor Interplay of Nd₂Sn₂O₇ Pyrochlore based Sensor in Selective Detection of Hydrogen, *J Electrochem Soc* 168 (2021) 047501. <https://doi.org/10.1149/1945-7111/ABF013>.

- [33] D. Varshney, A. Kumar, Structural, Raman and dielectric behavior in $\text{Bi}_{1-x}\text{Sr}_x\text{FeO}_3$ multiferroic, *J Mol Struct* 1038 (2013) 242–249. <https://doi.org/10.1016/J.MOLSTRUC.2013.01.065>.
- [34] A. Bhardwaj, A. Kumar, U. Sim, H.N. Im, S.J. Song, Synergistic enhancement in the sensing performance of a mixed-potential NH_3 sensor using $\text{SnO}_2@\text{CuFe}_2\text{O}_4$ sensing electrode, *Sens Actuators B Chem* 308 (2020) 127748. <https://doi.org/10.1016/J.SNB.2020.127748>.
- [35] X. Liu, J. Li, L. Guo, G. Wang, Highly Sensitive Acetone Gas Sensors Based on Erbium-Doped Bismuth Ferrite Nanoparticles, *Nanomaterials* 2022, Vol. 12, Page 3679 12 (2022) 3679. <https://doi.org/10.3390/NANO12203679>.
- [36] A. Kumar, M. Kumar, R. Kumar, R. Singh, B. Prasad, D. Kumar, Numerical modelling of Chemisorption of oxygen gas molecules on the surface of semiconductor for gas sensors applications, *Mater Today Proc* 18 (2019) 1272–1279. <https://doi.org/10.1016/J.MATPR.2019.06.589>.
- [37] N. Bârsan, Transduction in Semiconducting Metal Oxide Based Gas Sensors - Implications of the Conduction Mechanism, *Procedia Eng* 25 (2011) 100–103. <https://doi.org/10.1016/J.PROENG.2011.12.025>.
- [38] N. Barsan, U. Weimar, Conduction model of metal oxide gas sensors, *J Electroceram* 7 (2001) 143–167. <https://doi.org/10.1023/A:1014405811371>.
- [39] T.H. Wu, Y.M. Li, K.Y. Ni, T.K. Li, W.S. Lin, Vanadium oxides obtained by chimie douce reactions: The influences of transition metal species on crystal structures and electrochemical behaviors in zinc-ion batteries, *J Colloid Interface Sci* 608 (2022) 3121–3129. <https://doi.org/10.1016/J.JCIS.2021.11.040>.
- [40] A. Kumar, M. Kumar, R. Kumar, R. Singh, B. Prasad, D. Kumar, Numerical modelling of Chemisorption of oxygen gas molecules on the surface of semiconductor for gas sensors applications, *Mater Today Proc* 18 (2019) 1272–1279. <https://doi.org/10.1016/J.MATPR.2019.06.589>.
- [41] A. Rothschild, Y. Komem, On the relationship between the grain size and gas-sensitivity of chemo-resistive metal-oxide gas sensors with nanosized grains, *J Electroceram* 13 (2004) 697–701. <https://doi.org/10.1007/S10832-004-5178-8>.
- [42] F.U. Khan, S. Mehmood, X. Zhao, Y. Yang, X. Pan, Ultra-sensitive bimetallic alloy loaded with porous architecture MOF for ammonia detection at room temperature, in: *Proceedings - IEEE International Symposium on Circuits and Systems*, Institute of Electrical and Electronics Engineers Inc., 2021. <https://doi.org/10.1109/ISCAS51556.2021.9401554>.
- [43] T. Gro, H. Duda, J. Krok-kowalski, J. Walczak, E. Filipek, P. Tabero, A. Wyrostek, K. Barner, Electrical and optical properties of AVO_4 ($\text{A} = \text{Fe}, \text{Cr}$,

- Al) compounds, [Http://Dx.Doi.Org/10.1080/10420159508226277](http://dx.doi.org/10.1080/10420159508226277) 133 (2006) 341–348. <https://doi.org/10.1080/10420159508226277>.
- [44] V. Katari, S.J. Patwe, S.N. Achary, A.K. Tyagi, High Temperature Structural, Dielectric, and Ion Conduction Properties of Orthorhombic InVO₄, *Journal of the American Ceramic Society* 96 (2013) 166–173. <https://doi.org/10.1111/J.1551-2916.2012.05447.X>.
- [45] V.D. Nithya, R. Kalai Selvan, Synthesis, electrical and dielectric properties of FeVO₄ nanoparticles, *Physica B Condens Matter* 406 (2011) 24–29. <https://doi.org/10.1016/J.PHYSB.2010.10.004>.
- [46] N. Barsan, U. Weimar, Conduction model of metal oxide gas sensors, *J Electroceram* 7 (2001) 143–167. <https://doi.org/10.1023/A:1014405811371>.
- [47] Z. Zhang, J.T. Yates, Band bending in semiconductors: Chemical and physical consequences at surfaces and interfaces, *Chem Rev* 112 (2012) 5520–5551. <https://doi.org/10.1021/cr3000626>.
- [48] M. Hübner, C.E. Simion, A. Tomescu-Stănoiu, S. Pokhrel, N. Bârsan, U. Weimar, Influence of humidity on CO sensing with p-type CuO thick film gas sensors, *Sens Actuators B Chem* 153 (2011) 347–353. <https://doi.org/10.1016/J.SNB.2010.10.046>.
- [49] J. Dhakshinamoorthy, B. Pullithadathil, New Insights Towards Electron Transport Mechanism of Highly Efficient p-Type CuO (111) Nanocuboids-Based H₂S Gas Sensor, *Journal of Physical Chemistry C* 120 (2016) 4087–4096. <https://doi.org/10.1021/acs.jpcc.5b11327>.
- [50] J. Hu, D. Li, J.G. Lu, R. Wu, Effects on electronic properties of molecule adsorption on CuO surfaces and nanowires, *Journal of Physical Chemistry C* 114 (2010) 17120–17126. <https://doi.org/10.1021/jp1039089>.
- [51] B. Lyson-Sypien, M. Radecka, K. Świerczek, B. Lyson-Sypien, M. Radecka, M. Rekas, K. Swierczek, K. Michalow-Mauke, T. Graule, K. Zakrzewska, Grain-size-dependent gas-sensing properties of TiO₂ nanomaterials, *Elsevier* 211 (2015) 67–76. <https://doi.org/10.1016/j.snb.2015.01.050>.
- [52] A. Reghu, L.J. Legore, J.F. Vetelino, R.J. Lad, B.G. Frederick, Distinguishing Bulk Conduction from Band Bending Transduction Mechanisms in Chemiresistive Metal Oxide Gas Sensors, *Journal of Physical Chemistry C* 122 (2018) 10607–10620. <https://doi.org/10.1021/acs.jpcc.8b01446>.

List of Figures

| | |
|--|----|
| Figure 1.1: The gas concentration detecting range of many typical gas sensors. | 5 |
| Figure 4.1: Inkjet printed Interdigit on polyimide foil for gas sensing. | 10 |
| Figure 4.2:(a) Schematic of prefabricated sensor and interdigit motif for sensor (above) (b) coated ceramic and flexible inkjet printed sensor before and after growth (below) | 11 |
| Figure 4.3: The sensors (left to right) Ceramic fabricated sensor, flexible substrate and a reference sensor with the required electronics. | 11 |
| Figure 4.4: (Top to bottom) “ON/OFF” testing by alternating between a beaker with saturated ethanol vapours and an empty beaker, Schematic of the gas sensing chamber and an image of the lid (overview) | 13 |
| Figure 4.5: Inkjet formulation space graph using Reynolds and weber numbers based on [29] Brian Derby (A) Droplet formation as seen from the fiducial camera (B). | 14 |
| Figure 4.6: Gas sensing responses from the on/off testing (above) and gas chamber testing (below). | 16 |
| Figure 4.7: Observed gas sensing responses for ZnO nanoforest sensor. | 17 |
| Figure 4.8: Observed gas sensing responses for polymer drop casted sensor. | 17 |
| Figure 5.1: Schematic of the gas sensing system (above) and the sensing chamber with the sensor holder with the chamber lid (below). | 19 |
| Figure 5.2: Transient response curves of BSFO (a) Repeatability towards 2 ppm of NO ₂ at operating temperature; (b) Dynamic sensing characteristics to different concentration of NO ₂ at operating temperature [DD1]..... | 22 |
| Figure 5.3: (a) Response/recovery dynamics (b) Logarithmic dependency for the BSFO sensor. [DD1]..... | 23 |
| Figure 5.4: Cross sensitivity test for BSFO at operating temperature. [DD1] | 24 |
| Figure 6.1: Transient response curve of repeatability towards NH ₃ [DD2] | 26 |
| Figure 6.2: Dynamic sensing characteristics to different concentration of NH ₃ at operating temperature [DD2]..... | 27 |
| Figure 6.3: LOD analysis from optimal sensing curve of CrVO ₄ sensor [DD2]. ... | 28 |
| Figure 6.4: (a) Response/recovery dynamics (b) Logarithmic dependency for the CrVO ₄ sensor [DD2]..... | 29 |
| Figure 6.5: Cross sensitivity testing for CrVO ₄ sensor. | 30 |
| Figure 6.6: The change in induced band bending ($q\Delta V$) over NH ₃ gas concentration [DD2]. | 32 |
| Figure 6.7: Band bending (a) in the presence of atomic oxygen species (b) in the presence of ammonia towards our CrVO ₄ sensor [DD2]. | 32 |

List of Tables

| | |
|---|----|
| Table 1 ZnO Nanorods growth solution (PEI concentration varies for control) | 11 |
| Table.2 Seed layer ink properties and generated dimensionless values | 14 |

List of Symbols, Units, Abbreviations and Acronyms

| | |
|--------------------|--|
| Θ | Contact angle |
| cm | Centimetre |
| nm | Nanometre |
| cP | Centipoise |
| % | Percentage |
| MEMS | Micro-Electro-Mechanical Systems |
| μm | Micrometre |
| CIJ | Continuous Ink-jet |
| DOD | Drop-on-Demand |
| pH | The decimal logarithm of the reciprocal of the hydrogen ion activity |
| $^{\circ}\text{C}$ | Degrees centigrade |
| LED | Light emitting diode |
| SEM | Scanning electron microscope |
| γ | Surface Energy |
| <i>wt</i> | Weight |
| mPa-s | Milli pascal second |
| kg/m ³ | Kilogram per meter cube |
| mN/m | Milli newton per meter |
| DNA | Deoxyribonucleic acid |
| $\mu\Omega$ | Micro Ohm |
| DMP | Dimatix Materials Printer |
| ppm | Parts per million |
| 3-D | Three dimensional |
| PI | Polyimide |
| PTMSDPA | poly[1-phenyl-2-[p-(trimethylsilyl)phenyl]acetylene] |

Curriculum Vitae

Name: David John Dmonte
Date of birth: 28th January 1995
Place of birth: Chennai, India
Permanent address: B-102, Urbanvilla Apts, no 304/45B, Velachery main road, Chennai, Tamilnadu, 600042, India
Affiliation: Centre of Polymer Systems, Tomas Bata University in Zlín, třída Tomáše Bati 5678, 760 01 Zlín, Czech Republic
E-mail: dmonte@utb.cz
Education: **2018 – to date**
Tomas Bata University in Zlin, Centre of Polymer Systems, Ph.D. studies in Nanotechnology and Advanced Materials
2012 – 2017
Karunya University, Coimbatore, 641114, India
Integrated M.Sc. Nanoscience and Technology,
Projects: **Internal funding**

- IGA/CPS/2018/007- Development and studies of conductive nanomaterial for polymer electronics – Member of research team.
- IGA/CPS/2019/007- Development and study of nanostructure material in gas sensing system – Member of research team.
- IGA/CPS/2020/003- Preparation and characterization of doped nanostructures for gas sensing applications - Member of research team.
- IGA/CPS/2021/002- Preparation and characterization of doped nanostructures for gas sensing applications - Member of research team.
- IGA/CPS/2022/002 Preparation, characterization and gas sensing of nanostructures for gas sensing applications - Member of research team.-
- IGA/CPS/2023/006- Preparation, characterization and gas sensing of nanostructures for gas sensing applications - Member of research team.--

External funding

NPU I LO1504 – Centre of Polymer Systems plus (2018-2020) – Research Project Staff

Project GAČR 19-23647S (2019-2021) – Research Project Staff

The European Union's Horizon 2020 research and innovation programme under grant agreement No 739566

VEGA 1/0844/21 project granted by the Slovak Research and Development Agency

ERASMUS+ programme – Host - The University of Cologne

Research Output

1. Dmonte, David John; Šuly, Pavol; Antoš, Jan; Urbánek, Pavel; Kuřitka, Ivo; ,Inkjet printing of a gas sensor,NANOCON Conference Proceedings-International Conference on Nanomaterials,,,,2020,TANGER Ltd.
2. Dmonte, David John; Bhardwaj, Aman; Wilhelm, Michael; Fischer, Thomas; Kuřitka, Ivo; Mathur, Sanjay; ,Sub PPM Detection of NO₂ Using Strontium Doped Bismuth Ferrite Nanostructures, Micromachines,14,3,644,2023, MDPI
3. Dmonte, David John; Bhardwaj, Aman; Kavraz, Pelin; Slobodian, Rostislav; Antos, Jan; Sisman, Orhan; Galusek, Dusan; Fischer, Thomas; Mathur, Sanjay; Kuritka, Ivo; Detection of NH₃ gas using CrVO₄ nanoparticles, Sensors and Actuators B: Chemical, 135380, 2024, Elsevier

David John Dmonte, M.Sc., Ph.D.

**Preparation and characterisation of nanostructured materials for
electronic gas sensor devices**

Příprava a charakterizace nanostrukturovaných materiálů pro elektronická
čidla senzorů plynů

Doctoral Thesis Summary

Published by: Tomas Bata University in Zlín,
nám. T. G. Masaryka 5555, 760 01 Zlín.

Edition: published electronically

Typesetting by: David John Dmonte, M.Sc., Ph.D.

This paper has not undergone any proofreading or editorial review

Publication year: 2024

First Edition

ISBN 978-80-7678-264-8